inorganics

MDPI

Review

Multi-Dimensional Inorganic Electrode Materials for High-Performance Lithium-Ion Batteries

Musab Hammas Khan *, Patrizia Lamberti and Vincenzo Tucci

Department of Information and Electrical Engineering and Applied Mathematics, University of Salerno, Via Giovanni Paolo II, 132, 84084 Fisciano, SA, Italy; plamberti@unisa.it (P.L.); vtucci@unisa.it (V.T.)
* Correspondence: muskhan@unisa.it

Abstract: Energy storage devices are essential for enhancing the effectiveness and sustainability of electrical energy. Lithium-ion batteries (LIBs) are one of the most efficient energy storage solutions available. The choice of electrode materials plays a vital role in defining the performance of an energy storage device. A range of electrode materials have been developed utilizing both organic and inorganic substances. Due to their notable electrochemical characteristics, strong chemical stability, and well-established technological approaches, inorganic materials have been extensively studied to achieve high-performance devices. This review paper aims to provide a thorough and analytical review of different materials ranging from zero- to three-dimensional (3D), like quantum dots, nanotubes, and nanosheets that have been proposed for high-performance LIBs. This study also includes challenges and future pathways to address the issues with inorganic materials utilized as electrode materials for high-performance energy storage LIBs.

Keywords: batteries; inorganic electrode materials; lithium-ion batteries; 0D, 1D, 2D, and 3D nano-materials

check for updates

Academic Editor: Ting Deng

Received: 31 December 2024
Revised: 7 February 2025
Accepted: 10 February 2025
Published: 17 February 2025

Citation: Khan, M.H.; Lamberti, P.; Tucci, V. Multi-Dimensional Inorganic Electrode Materials for High-Performance Lithium-Ion Batteries. *Inorganics* **2025**, *13*, 62. https://doi.org/10.3390/inorganics13020062

Copyright: © 2025 by the authors. Licensee MDPI, Basel, Switzerland. This article is an open access article distributed under the terms and conditions of the Creative Commons Attribution (CC BY) license (https://creativecommons.org/licenses/by/4.0/).

1. Introduction

Devices for energy storage are more and more diffusely applied across various domains, including electric power distribution, electronics, automotive, aerospace, etc. [1–3], for tackling the global challenges related to the finite availability of fossil fuels and to air pollution reduction.

Many different technologies have been proposed to fulfill the constraints of the required power and energy in such diversified domains. Fuel cells demonstrate significant energy density, yet they possess a relatively low power density. Supercapacitors have higher power but less energy densities and longer cycle lifetimes due to surface charge storage processes [4–6] whereas rechargeable batteries provide high energy densities as a result of the faradaic charge storage mechanism [7–10]. Among these last electrochemical systems, throughout the last three decades, lithium-ion batteries (LIBs) have been used as the power source for a variety of products, including electric vehicles, power tools, laptops, mobile phones, etc. As well as being lightweight, LIBs have the highest energy and power densities compared to the other battery technologies. They also have a long lifecycle and a low self-discharge rate, which makes them reliable and easy to maintain.

The three primary components of a LIB (as of any other battery) are an electrolyte and two electrodes (anode and cathode). The cathode stores ions when charging whereas the anode stores lithium ions during discharging. The presence of electrolytes in batteries enables the movement of ions between the anode and cathode, thereby ensuring efficient energy storage and release. The most commonly used liquid electrolytes employed in LIBs

are Lithium salts, like $LiPF_6$. Solid electrolytes, including those composed of ceramic or polymer, as well as gel electrolytes, represent two additional types of electrolytes. Each of these categories offers a distinct array of benefits, encompassing aspects such as safety and stability.

The electrodes significantly influence a battery's energy storage capacity, efficiency, and overall lifespan. During the charging and discharging processes, the anode and cathode are crucial for ion mobility, directly affecting the electric battery's overall performance. The choice of material influences ion storage capacity, conductivity, and stability during several charge-discharge cycles. Efforts are now underway to produce and use the most appropriate materials for electrode components in batteries.

Even though there have been improvements over the years, the best electrode materials for LIBs that use the intercalation mechanism have reached their peak performance. This is when lithium ions are reversibly incorporated into the structure of the host material. This implies that investigating novel materials or ion storage processes other than conventional intercalation may be necessary to achieve additional notable increases in energy capacity or efficiency. Because of this, a significant amount of attention has been focused on high-capacity conversion reaction-type cathodes, such as those containing sulfur (lithium-sulfur batteries) and oxygen (lithium-air batteries). Furthermore, safe and affordable rechargeable batteries hold great potential as workable alternatives for large electrical systems [11,12]. Promising potential for enhancing battery performance, such as cyclic stability, specific capacity, specific energy, and charge/discharge rate, has been shown for a variety of electrodes based on nanomaterials [13–16].

Nanomaterials with a significantly enhanced surface area markedly enhance ion storage and reaction speeds, increasing battery capacity and power output. Their nanoscale dimensions facilitate accelerated ion diffusion and more compact electron transport pathways, leading to enhanced efficiency. Furthermore, nanomaterials possess the potential to accommodate volumetric changes during cycling, thereby enhancing the longevity and stability of batteries. Nanoparticles can be categorized based on their size, shape, and structural morphology.

Researchers have made a lot of progress in the past few years in studying zero-dimensional (0D), one-dimensional (1D), two-dimensional (2D), and three-dimensional (3D) nanostructures like quantum dots, nanotubes, and nanosheets as high-performance electrode materials for energy storage devices. Even though they have a lot of interesting properties, problems like material aggregation, limited electrolyte diffusion, and slow reaction kinetics limit their applicability [17,18].

More than 15,000 publications in 2024 that seek the best electrode material for high-performance LIBs are on the Google Scholar website. We conducted this search in December 2024 using the keywords anode, cathode, and electrode materials for lithium-ion batteries. Based on the literature review, this study aims to analyze the characteristics of 0D, 1D, 2D, and 3D inorganic materials applied for LIB electrodes in an organized way. It focuses on their electrochemical properties, energy and power densities, and important performance metrics like charge transfer efficiency, capacity retention, and cycle stability. The presented results offer a wide-ranging overview of the pros, cons, and trade-offs of each dimensionality by showing how structural morphology affects energy storage mechanisms. This may provide a suitable reference for researchers engaged in designing long-lasting, high-performance energy storage systems.

2. Electrode Materials for Use in High-Performance ESD

The investigation of high-performance electrodes, electrocatalysts, and photoelectrodes stands as a pivotal element in the commercialization of these renewable energy

technologies. Considering that a battery functions as a dynamic chemical reactor, enhancing its performance through the use of high-performance materials necessitates a profound understanding of the processes occurring at every level. Novel electrode materials for Lithium-ion batteries, which are renowned for their exceptional cycle stability and appealing specific capacity, have drawn a lot of interest in recent years [19]. More than 15,000 publications in 2024 that seek the best electrode material for high-performance LIBs are on the Google Scholar website. We conducted this search in December 2024 using the keywords anode, cathode, and electrode materials for lithium-ion batteries.

Typical materials for LIBs include carbon-based materials, metal oxides, conducting polymers, and different combinations of these elements as electrode components. In recent studies, anode materials for LIBs have encompassed carbon and carbon-based materials [20–23], metal oxides [24–26], nitrides [27,28], and carbides [29,30], along with their composites [31,32]. $LiCoO_2$ [33], $LiMnO_2$ [34], and transition-metal phosphates, especially olivine $LiFePO_4$ [35], exemplify layered compounds featuring an anion close-packed or very-close-packed lattice. They have garnered significant attention in both academic inquiry and commercial applications concerning cathode materials. Other materials that are widely utilized include conducting polymers. Electrodes adopted for high-performance energy storage devices include a variety of compounds for applications, such as carbonaceous compounds like graphene and carbon nanotubes [36,37], conducting polymers like PANI [38], metal oxides like MnO_2 [39], carbon nanocomposites [40,41], and metal oxide composites [42], among others. Inorganic materials hold considerable importance because of their ability to store lithium through a conversion mechanism [43]. Metals, in combination with carbon, like SnO_2 [44], Mo_2N [45], FeN [46], VN [47], Ni_3N [48], and NbN [49], have also been proposed as electrode materials due to the elevated specific energy and power densities, superior electrical conductivity, thermal stability, and electrochemical behavior.

2.1. Organic Electrode Materials

The swift advancement of OAMs necessitates collaborative efforts across various fields, including computer science, chemistry, and materials science. Organic electrode active materials provide a number of advantages, including their low cost, low impact on the environment, sustainability, adjustable design, and exceptional electrical storage activity. We can source these materials from biomass or produce them through straightforward synthesis methods [50,51]. A wide variety of batteries are available, such as lithium-ion, sodium-ion, aluminium-ion, magnesium-ion, and proton batteries, with considerable emphasis on the investigation of organic active materials (OAMs) [52]. In contrast to the rigidity of inorganic materials, the flexibility of organic materials renders them more suitable for bendable energy storage devices. However, achieving large-scale commercialization requires addressing several challenges [53,54]. At the moment, the main problems that OAMs face in the research field are low conductivity, the ability to dissolve in electrolytes, limited working current, low specific capacity, synthesis technology, and safety.

In particular, it is crucial to consider the safety of organic electrode materials. They exhibit significantly different thermal stability, making them more susceptible to inactivation at elevated temperatures [53].

2.2. Inorganic Electrode Materials

Although inorganic materials are the subject of the majority of the present research, interest in their wider potential in energy storage is growing due to their significant benefits, which include increased surface areas, superior electrical conductivity, enhanced thermal stability, greater number of active sites, and higher capacities compared to organic compounds [54]. A substantial array of inorganic materials serve as anode or cathode

materials for LIBs, with numerous reports available in the literature. The mechanism of their response enables them to be classified into three separate categories: alloying reaction (e.g., Si and Sn), intercalation reaction (e.g., $Li_4Ti_5O_{12}$), and conversion reaction (e.g., MnO and Fe_2O_3) [55,56].

Silicon has a very high specific capacity of 4200 mA h g^{-1} due to a 4.4-electron alloying reaction. It also has a very low operational voltage of about 0.4 V compared to Li/Li^+ [56]. Phosphorus (P) is an interesting anode material because it has a theoretical specific capacity of 2595 mA h g^{-1}. This comes from the reaction of 3Li + P ↔ Li3 P. Metal oxides exhibit high experimental and theoretical specific capacities, as documented in numerous studies [57,58]. Over the past 10 years, according to data available on Google Scholar, more than 50,000 have been published on inorganic electrode materials for lithium-ion batteries. The cathode material serves as a fundamental element that directly influences the overall performance of batteries. Inorganic cathode materials have garnered significant interest, primarily due to their impressive discharge capacity. The metallic elements typically exhibit accessible oxidation states (e.g., $Mn^{2+}/Mn^{3+}/Mn^{4+}$, $V^{3+}/V^{4+}/V^{5+}$, and $Fe^{2+}/Fe^{3+}/Fe^{4+}$), resulting in multi-electron reactions throughout the charge and discharge cycles. The Li_2FeSiO_4 (LFSO) material is cheap and good for the environment. It can help with a two-electron reaction that has a theoretical specific capacity of 332 mA h g^{-1} [59]. Newly discovered materials, like P14AQ/CNT nanocomposite and Triplite $LiFeSO_4F$ [60], have a lot of potential as cathodes.

Many inorganic nano-materials have been thoroughly investigated as LIB electrode materials, including metal oxides, metal phosphides, and oxysalt nanoparticles. The tiny size of these nanoparticles enables a reduction in the collective electrode tension (mechanical stress/strain) resulting from Li insertion/removal and the diffusion channel between lithium ions. Nevertheless, a significant issue with these nanoparticles is their comparatively poor conductivity, particularly when they are in weak contact [61–63].

3. Nanostructured Inorganic Electrode Materials

In the sequel, the classification proposed by Pokropivny and Skorokhod for NSMs [64], encompassing 0D, 1D, 2D, and 3D NSMs, is adopted. The advancements observed in recent years indicate that NSMs possess significant potential for the innovation of new technologies aimed at meeting the enduring demand for energy. But there are still constraints on using different types of nanostructures with different properties.

Zero-dimensional (0D) nanostructures like quantum dots are strongly reactive with a quick ion exchange that is made possible by high surface-to-volume ratios, although charge transport may be hampered by their poor connectivity. Additionally, 1D materials are perfect for enhancing conductivity in energy devices because they provide continuous channels for the passage of electrons and ions. Two-dimensional materials in layered structures provide huge surface areas and high ion diffusion rates, which are essential for energy storage in batteries and supercapacitor electrodes. Additionally, 3D materials show a stability and energy storage capacity enhanced by porous structures that optimize surface area and facilitate effective molecular movement. Every dimensionality has a distinct contribution and customized morphologies are becoming more and more important for high-energy storage devices [64]. Figure 1 illustrates the diverse dimensions of categorized nanomaterials [65].

Table 1, Shows a summary of some relevant properties of nanomaterials with different sizes (0D, 1D, 2D, and 3D) used in LIBs. This comparison underscores the possible advantages of each solution in enhancing electrochemical performance and energy storage efficiency. Due to their unique structural properties, 0D and 3D materials often have high initial capacities in some cases. However, they often face problems like poor cycling stability, agglomeration (in 0D), and inefficient ion diffusion (in 3D). These problems arise because

of shape restrictions, such as particle aggregation, volume expansion, and limited access to electrolytes. In contrast, 1D and 2D materials typically offer a better balance of capacity, cycle life, and rate performance due to their optimized morphology for ion transport and structural integrity. Therefore, a material's suitability for lithium-ion batteries depends not only on how much power it can hold but also on how well it can keep working repeatedly and in real-world situations.

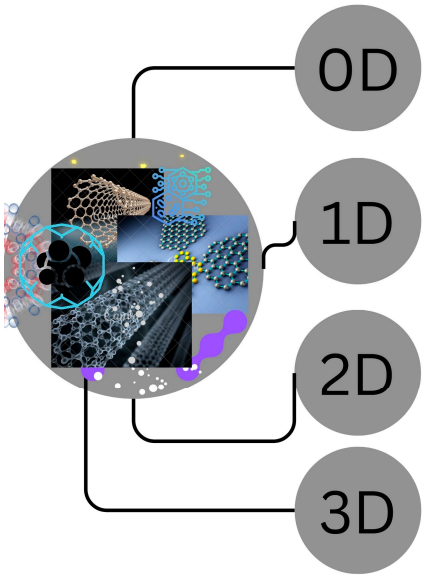

Figure 1. Different possible dimensions of the nanomaterials.

Table 1. Zero to Three Dimensional inorganic nano-materials materials with their characteristics for high-performance LIBs.

Material	Capacity (mA h g^{-1})	Specific Current (mA g^{-1})	No. of Cycles	Reference
0D materials				
TiO_2@GNRs	320.8	100	500	[66]
NiO@Co_3O_4@GQDs	1158	100	250	[67]
SnO_2-GNS	793	400	150	[68]
$Ca_3Co_4O_9$	316.3	-	100	[69]
Si QDs	1232	200	100	[70]
SnO_2/Graphene	635	60	100	[71]
ZnO@ZnO QDs/C NRAs	699	500	100	[72]
SnO_2/graphene composite	634	100	50	[73]
MoS_2@CNT Fabric	700	100	50	[74]
SnO_2/GNS	570	50	30	[75]
GNS/Fe_3O_4	1026	35	30	[76]
1D materials				
Ge-CNFs	281.6	5000	5000	[77]
Si	1200	2000	500	[78]
$ZnMnO_3$	950	500	500	[79]
$Li_{1.2}Ni_{2.5}B_2$	350	100	500	[80]
S@$Sr_8Ti_7S_{21}$	1315	260	400	[16]
Fe_2O_3	812	100	300	[81]
$ZnCo_2O_4$	1050	400	200	[82]
Co_3O_4	1800	300	100	[83]

Table 1. *Cont.*

Material	Capacity (mA h g^{-1})	Specific Current (mA g^{-1})	No. of Cycles	Reference
Cu-Si	1500	1400	100	[84]
SnO_2-CuO	600	500	100	[85]
Zn_4Sb_3	450	100	100	[86]
Nb_2Se_9	542.2	100	100	[87]
2D materials				
Cu_3Si/Si	1675	200	100	[15]
NPCN/Si-2	1977	100	100	[13]
Graphene/MoS_2 composite	1351	100	200	[88]
Si nanosheets/graphene composite	1650	840	50	[89]
Co_3Sn_2/Co–N-doped graphene composite	1615	2501	100	[90]
MoO_2/carbon	1051	500	100	[91]
Si–reduced graphene oxide composite	1500	1350	100	[92]
SiA/NC anode	1224	20	100	[93]
Si/graphene composite	1390	2000	200	[94]
Graphene/$NiCo_2O_4$	1267	100	10	[95]
FeS-rGO composite	978	100	40	[96]
3D materials				
Rutile TiO_2	140	75	1000	[97]
$Cs_2NaErCl_6$	120	300	500	[98]
$CsPbBr_3$@CNTs	470.2	100	200	[99]
$CsPbBr_3$	261	60	100	[100]
$CsPbI_3$	235	40	100	[101]
CoO QD/Graphene	1008	1000	50	[102]
Co_3O_4	866	178	50	[103]
CoO@3DOM	560.8	1000	50	[104]
$Cs_2NaBiCl_6$	775	75	25	[105]
$CsPbCl_3$	612.3	50	-	[106]

3.1. Zero-Dimensional Inorganic Electrode Materials

Zero-dimensional (0D) materials are defined as structures whose dimensions are less than 100 nm on all three sides. These include nanoparticles shaped like onions, spheres, and cages, as well as quantum dots. These structures may provide useful surfaces for electrochemical activity because of their specific dimensions [107]. Published literature extensively covers zero-dimensional electrode materials and the blending of 0D nanoparticles with other materials for use as LIB electrode materials. The electrochemical characteristics of zero-dimensional materials are highlighted, with particular attention paid to specific capacity, current density, and cyclic performance. Their usefulness and potential for use in cutting-edge energy storage systems are shown by this viewpoint.

Using co-precipitation and molten salt methods, Wang et al. created the zero-dimensional anode material $Ca_3Co_4O_9$, which works very well in LIBs. The 0D polyhedron anode had a high initial charge capacity of 391.9 mA h g^{-1}. It maintained 316.3 mA h g^{-1} with more than 95% Coulombic efficiency after 100 cycles. The material had a lot of surface area and ion channels that helped lithium ions (Li^+) move through it. This makes the capacity 33% higher at five rates. This material proved that micro/nanostructure engineering may enhance cycle stability and rate performance [69].

Choi et al. showed that the π-conjugated molecule had better electrochemical performance. They found that the silicon quantum dot (Si QD), a bridge structure, could discharge at the value of 1957 mA h g^{-1} initially and keep 63% of its capacity after 100 cycles at a rate of 200 mA g^{-1}. The π-conjugated molecules can make the electrochemical performance of

the material better. They protect electrical conductivity and structural integrity from the mechanical stress that comes from the alloying process. The structure of the Si QD cluster improves stability and ion transport, which makes the cycle stability better than with Si QDs that are not clustered. By adding functional groups and altering organic structures, Si QD clusters' electrochemical properties may be further improved. This approach has significant promise for enhancing the anode materials in high-performing lithium-ion batteries [70]. According to Chen et al. [108], there are numerous dead zones internally present during the fabrication of a material that essentially remains inactive in terms of electrochemical activity. The diffusion depth of an electrolyte is limited to approximately 20 nanometres. It has been demonstrated that quantum dot (QD) structures can offer the necessary small size and a large specific surface area with a specific pore structure, both of which are crucial for improving performance and covering all relevant zones. They synthesized $NiCo_2S_4$ quantum dots and applied them onto nickel foam. After CV tests, it was clear that the material $NiCo_2S_4$ exhibits a larger CV area compared to the CoS_2 and NiS_2 in the KOH electrolyte. The GCD analysis revealed the specific charge capacity (calculate the precise charge that a material can deliver or store in relation to its mass) of $NiCo_2S_4$ was 987.2 C g^{-1}, which was greater than CoS_2 and NiS_2. They also constructed and tested a real two-electrode device that consists of nitrogen-doped reduced graphene oxide nanosheets used as the anode material and $NiCo_2S_4$ as the cathode material. The real device reached a value of 168.1 F g^{-1} specific capacitance at a low specific current of 1 A g^{-1}. The GCD curves have almost symmetric charge-discharge branches and a small potential drop. This suggests that the capacitance is very reliable. The cyclic examination of the device demonstrated a stability level of 91.9% after 15,000 cycles. This real device demonstrated a high energy density and power density of 67.5 W h kg^{-1} and 850 W kg^{-1}, respectively [108].

Wang et al. [109] created and tested a core-shell heterogeneous nanoparticle structure with a carbon shell around a $LiFePO_4$ core. This composite demonstrated a value of 169 mA h g^{-1} of specific capacity at a 0.6 C discharge rate, which was almost equal to the theoretically reported values for $LiFePO_4$. It maintained a reasonable specific capacity of 90 mA h g^{-1}, even when discharged at a high rate of 60 C. Furthermore, the material's cyclic ability was remarkable; after 1100 cycles at a discharge rate of 0.6, it had lost less than 5% of its specific capacity.

Oxide coatings, including MgO, Al_2O_3, and ZnO, have been added to LIB cathode materials to improve their performance. As a result, strain during phase transition may be reduced and the materials' structural stability can be enhanced. In their study, Ting and colleagues showed that a 10 nm layer of nanocrystalline ZnO may improve the $LiCoO_2$ cathode's electrochemical performance [110]. $LiCoO_2$, $LiNiO_2$, and $LiMn_2O_4$ are examples of electroactive cathode materials that may have oxide coatings applied to their surfaces to minimize phase transitions, enhance structural stability, and prevent electrolyte–cathode contact. It is evident in several additional instances that the coatings could be able to enhance conductivity [111].

Another kind of electrode material utilized in energy storage batteries is transition metal dichalcogenides. When 0D inorganic materials bind with organic ones, they may function effectively. Rana et al. synthesized CNTF/MoS_2, a zero-dimensional nanocomposite, for use as a battery electrode. Enhancing conductivity, diffusion, and cycle stability was the main goal. This technique uses MoS_2-coated carbon nanotube fibers (CNTFs) to make composite electrodes that do not need metallic collectors or polymer additives. The electrodes' excellent electrical conductivity and durability surpass those of conventional designs. They achieve a specific capacity of 0.7 Ah g^{-1} with retention rates of 108% after 50 cycles at a specific current of 0.1 Ag^{-1} and 89% after 250 cycles at a specific current

of 1 A g^{-1}. The flexible composite fabrics provide remarkable mechanical strength and consistent performance at varying current densities. However, CNTFs may be expensive and complicated to produce and process, which could prevent them from being widely used in certain applications. Furthermore, even though carbon nanotubes show remarkable performance metrics, issues with their long-term stability and environmental effects still need to be resolved [74].

When combined with two-dimensional materials, zero-dimensional materials may achieve remarkable results. Because of its large surface area and excellent electrical properties, which are crucial for energy storage, graphene is a popular electrode material. A significant mass of published information concerns graphene pairings with zero-dimensional inorganic materials. This 2D/0D, graphene/inorganic material combination has led to the development of several novel composite electrode material architectures [112]. These include several anode materials, like Co_3O_4 and SnO_2, and cathode materials, including sulfur (S), $LiFePO_4$, V_2O_5 [113–115], MoO_2 [116], NiO [117], Si [118], Ge [119], and more.

Li et al. applied SnO_2 onto graphene in a structurally and morphologically controlled manner via atomic layer deposition [68]. They used the amorphous SnO_2 as an anode material for the real device testing. As a result, the recorded capacity was 793 mA h g^{-1} after 150 charge-discharge cycles. Over graphene nanosheets, Kim et al. decorated SnO_2 nanoparticles and created a SnO_2/graphene composite for enhancing the LIB performance [73]. In comparison to simply mixed samples, the produced composite showed better electrochemical performance. After 50 charge-discharge cycles, the material showed a specific capacity of 634 mA h g^{-1}, which was due to the uniformly distributed symmetry of nano particles. A one-step hydrothermal method was developed by Wang et al. to synthesize graphene–SnO_2 nanocomposites [71]. After 100 cycles, the generated nanocomposite showed remarkable rate capability and a 635 mA h g^{-1} specific capacity. SnO_2 nanoparticles were combined with graphene nanosheets by Paek et al., showing noticeably improved lithium storage performance [75]. After 30 cycles, the produced 2D/0D graphene–SnO_2 nanocomposite maintained a charge capacity of 570 mA h g^{-1}.

There are a lot of inorganic materials being used as an anode material of the LIBs. A straightforward two-step production of a graphene–Fe_2O_3 composite using the homogeneous precipitation of $FeCl_3$ was first reported by Zhu et al. [120]. They used a graphene composite for increasing the performance of LIBs, which showed an excellent cycle performance of 1355 and 982 mA h g^{-1} for discharge and charge capacities, respectively, depending on the mass of Fe_2O_3. There is also reported Mn_3O_4 material by Wang et al., who demonstrated that the material achieved a high specific capacity value of 810 mA h g^{-1} at the specific current value of 40 mA g^{-1}. The obtained capacity value was in the range of Mn_3O_4's theoretical capacity [76].

In storage applications, the morphology of the material is very important and may impart, unlike electrochemical behaviour. Figure 2 shows various 0D materials: SEM images highlight unique morphologies whereas cycling tests lead to different performances. The MoS_2 coating, with its nanoscale thickness (7–80 nm), exhibits 0D characteristics when analyzed independently but integrates into a 1D CNT-based hybrid system, forming a continuous conformal layer (Figure 2a). The large surface area of 0D MoS_2 helps ions move around better and the structural stability of 1D CNTs helps electrons move around better. This makes for a high capacity and great cycling performance (Figure 2b). Similarly, the amorphous SnO_2-GNS composite, with its 0D morphology of 3–5 nm nanoparticles, maximizes the electrolyte contact area, improving ion transport and capacity (Figure 2d). The isotropic structure of this battery responds well to changes in volume during cycling. This keeps the structure stable and gives it a high capacity of 793 mA h g^{-1} (Figure 2e). This makes it better than larger crystalline SnO_2 nanoparticles (30–40 nm), which have

trouble adapting their structure (Figure 2c). The SnO_2/graphene composite has even more of the benefits of a 0D shape. The main SnO_2 nanoparticles are about 4 nm wide and spread out evenly on the graphene (Figure 2f). This makes it easier for ions to move through and for electrochemical reactions to happen. These small particles stick together to make bigger structures (about 14 nm), which keeps the capacity and stability in check (Figure 2g). After 50 cycles, they have a reversible capacity of 634 mA h g^{-1} and a 98% coulombic efficiency (Figure 2h). Finally, Si quantum dots (Si QDs) have a 0D shape that gives lithium ions a lot of surface area to interact with. The π-conjugated molecules around the material act as a buffer layer, reducing the mechanical stress caused by changes in volume and making it easier for electrons and Li^+ to move around (Figure 2i,j). This is what lets the material keep about 63% of its capacity (1232 mA h g^{-1}) after 100 cycles (Figure 2k). These studies collectively emphasize how 0D morphologies—whether as independent nanoparticles, integrated into hybrid systems or combined with secondary structures—play a pivotal role in maximizing electrochemical performance by enhancing surface area, ion transport, and structural stability. Due to their small size, 0D materials often generate a lot of aggregation and poor connectivity, which limits the routes that ions and electrons may take. To make matters worse, when 0D materials are often cycled (charge/discharge), they may lose their stability.

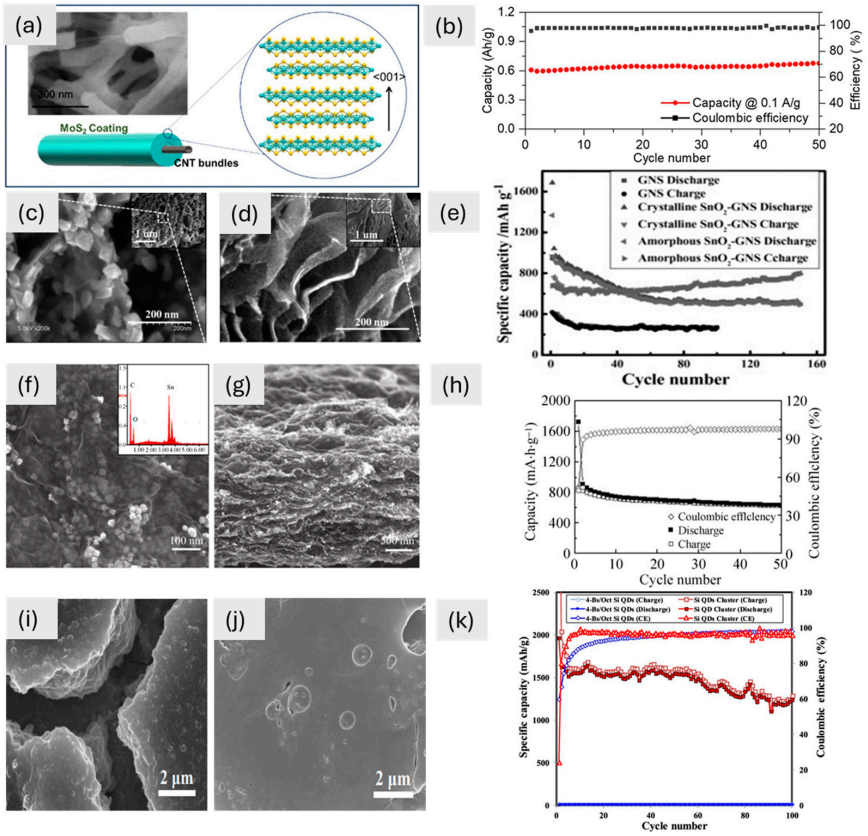

Figure 2. (**a**) Field emission SEM image of the CNTF/MoS_2 composite and a schematic picture of the MoS_2 coating around the CNTF bundles, with an inset showing a magnification; (**b**) cyclic performance of composite at 0.1 A g^{-1} [74]. Copyright © 2021 American Chemical Society. SEM images of (**c**) crystalline SnO_2-GNS, (**d**) amorphous SnO_2-GNS, (**e**) cycle performance at different rates but the same potential window of 0.01–3.00 V for GNS (100 mA g^{-1}) and for crystalline and amorphous SnO_2-GNS (400 mA g^{-1}) [68]. Copyright © 2012 Wiley. (**f**) SnO_2/graphene SEM image at 100 nm, with an inset of the energy spectrum, (**g**) SEM image (500 nm) of the composite, and (**h**) cyclic performance of SnO_2/graphene at a rate of 100 mA g^{-1} [73]. Copyright © 2010 Springer. SEM images of (**i**) 4-Bs/Oct Si QDs and (**j**) Si QD cluster and (**k**) galvanostatic cycling of Si QD cluster [70]. Copyright © 2020 American Chemical Society.

3.2. One-Dimensional Inorganic Electrode Materials

Unlike 0D nanostructures, 1D nanomaterials allow for effective charge transfer along their micro-scale axis by a direct conduit. Owing to their unique benefits, 1D nanostructures have been largely investigated for possible application in electrochemical energy storage systems [21,121–126]. With a lot of ongoing research, these kinds of materials are being employed commercially for high-performance energy storage systems. We have chosen to present 1D inorganic materials based on their electrochemical performance related to their energy outputs. This approach highlights their potential as high-performance electrode materials for energy storage applications.

Yan et al. successfully coated SnO_2 nanowires with amorphous MnO_2 through the straightforward method of immersing them in a hot $KMnO_4$ solution [127]. The material showed a high value of specific capacitance (637 F g^{-1}) at a scan rate of 2 mV s^{-1}. This material also performed well in terms of energy density and power density; the reported values are 35.4 Wh kg^{-1} and 25 kW kg^{-1}, respectively. A one-dimensional nanostructured composite of manganese dioxide and polypyrrole was synthesized by Li et al. [128]. Following 500 cycles (charging/discharging) in an electrolyte, the composite demonstrated a specific capacitance of 320 Fg^{-1} within the potential range of 0.4–0.6 V. In another published paper by Chen et al. [129], a capacity of 185 mA h g^{-1} is reported for nanotubes composed of $LiCoO_2$, which is greater than the typical value of 140 mA h g^{-1}; for such material at higher cycle rates, its capacity quickly decreases.

Plenty of polyanionic compounds have been studied on a large scale due to their high theoretical specific capacities and stability, i.e., $LiFePO_4$, $LiMnPO_4$, $Li_3V_2(PO_4)_3$, and others [130–132]. $LiFePO_4$, $LiMnPO_4$, and $Li_3V_2(PO_4)_3$ can be made to work better with other types of nanomaterials by studying their one-dimensional morphologies. This is a revolutionary way to make lithium-ion batteries work better, even in hybrid materials, as shown in Figure 3. These structures greatly lower internal resistance by making continuous paths for ionic and electronic conduction. They also make it easier for lithium ions to move around quickly, which is important for high-rate capability. This shape also provides mechanical integrity, which effectively reduces problems related to volume expansion and contraction during cycling. This makes sure that the battery lasts a long time and works reliably. Ultimately, the strategic balance of a high surface area with superior conductivity not only optimizes electrochemical performance but also paves the way for next-generation energy storage solutions that meet the demands of modern technology.

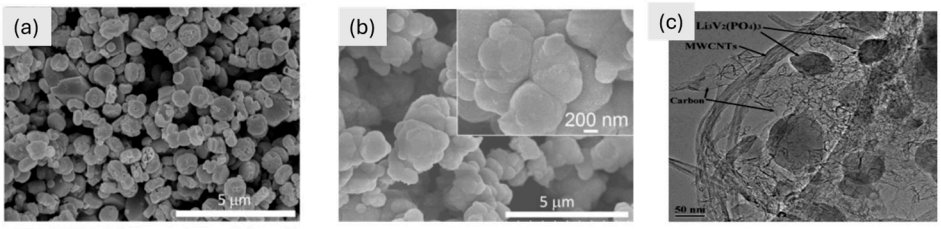

Figure 3. (**a**–**c**) SEM images of (**a**) $LiFePO_4$ and (**b**) $LiMn_{0.1}Fe_{0.9}PO_4$ at two different magnifications [133]. Copyright © 2021 scientific reports. (**c**) TEM image of the composite $Li_3V_2(PO_4)_3$/(C + MWCNTs) at 50 nm [134]. Copyright © 2011 ScienceDirect.

A hierarchical-structure $Li_3V_2(PO_4)_3$/C mesoporous nanowire was fabricated by Wei et al., which included uniformly implanted $Li_3V_2(PO_4)_3$ nanocrystals that maintained close contact with conductive carbon scaffolds [130]. Compared to regular LVP particles covered in carbon, these mesoporous nanowires showed better performance in terms of rate and cycle. The mesoporous nanowires retained 80% of their capacity even after 3000 cycles.

Nanofiber nanorod-structured Fe_2O_3-C was created by Kang and colleagues for use as electrode material in high-performance energy storage devices [81]. These nanofibers consist of nanosized hollow Fe_2O_3 spheres evenly distributed throughout the amorphous carbon nanofiber matrix. The improved rate and cycling performance were a consequence of the combination of the carbon matrix's continuous electron transport and the hollow nanospheres' ability to accept the volume shift that happens during cycling. This material shows a value of 812 mA h g^{-1} reversible capacity at a specific current of 1.0 A g^{-1} after 300 charge-discharge cycles.

Theoretically, silicon is another promising candidate for use in energy storage devices with high-capacity values of 4200 mA h g^{-1}. However, using Si material in lithium-ion batteries presents several challenges, such as the large volume variation (>300%) during lithiation/delithiation processes (removal and insertion of lithium-ions during charge-discharge), rapid capacity loss, and unstable SEI (Solid Electrolyte Interphase) layers. Furthermore, since Si is a semiconductor, its electronic conductivity is rather low. New research has found that mesoporous carbon nanofibers mixed with silicon nanoparticles or silicon nanofibers themselves work better for cycling and rate than silicon nanowires or particles in bulk. Hollow Si nanotubes may be used to achieve high performance [135]. Cui et al. presented the electrochemical characteristics of silicon nanowires [136]. These silicon nanowires have achieved a value of 1000 mA h g^{-1} and, even after 1000 charge-discharge cycles, they perform very well. Wu et al. [137] created a double-walled Si-SiOx nanotube structure. During lithiation, a stable outer SEI layer formed, enabling the expansion of the inner Si into the hollow region. Cycling performance was better with this SEI layer than with Si nanowires and nanotubes because it was thin and stable. Even after 6000 cycles and when tested at a high rate of 12, the capacity remained unchanged.

Wei et al. optimized $Li_{1.2}Ni_{2.5}B_2$ for use as an anode material for high-performance LIBs. This material shows outstanding stability during 500 charge-discharge cycles. Additionally, this anode material showed an excellent reversible capacity of 350 mA h g^{-1} at a current of 0.1 A g^{-1}. The results show that the 1D Ni/B structure is very promising as a commercially available LIB anode with the ability to charge quickly [80]. Dawei et al. presented the findings of a quasi-1D hexagonal chalcogenide perovskite material, $Sr_8Ti_7S_{21}$. The theoretical results of density functional theory showed that $Sr_8Ti_7S_{21}$ forms strong bonds with lithium polysulfides (LiPS). The effective sulfur host may circumvent the constraints. Consequently, S@$Sr_8Ti_7S_{21}$-based cathodes show a remarkable cycling stability of a 1315 mA h g^{-1} capacity over 400 cycles at 0.2 [16].

Woosung et al. reported an anode material (Nb_2Se_9) for Li-ion batteries (LIBs). This electrode exhibited a reversible specific capacity of 542.2 mA h g^{-1} when it was tested at a current rate of 0.1 A g^{-1} over one hundred cycles. Then, after the increase of specific current up to 3.2 A g^{-1}, further, it shows 272 mA h g^{-1} of capacity [87]. Tian et al. developed the Ge-CNF material specifically for use in high-performance energy storage devices. Nanotechnology and carbon coating modified this germanium/carbon nanofiber to enhance the LIBs' capacity and charging speed. This material was very durable and had excellent electrochemical properties. It could hold the capacity of 281.6 mA h g^{-1} after 5000 cycles (charging/discharging) at the specific current of 5 A g^{-1} and 795.9 mA h g^{-1} after 100 cycles at 0.1 A g^{-1}, with a coulombic efficiency of 99.76% [77].

The examination of TEM images, alongside cyclic performance data, reveals a compelling narrative about the intricate relationship between the morphologies of 1D materials and their electrochemical behaviors (Figure 4). The TEM image shows that $Sr_8Ti_7S_{21}$ perovskite has a flat structure (Figure 4a). The hexagonal Sr framework shows how well it is aligned, which improves lithium polysulphide binding and redox kinetics. This leads to a high capacity and great cycling stability, with only 0.08% decay over 400 cycles (Figure 4b).

Fe_2O_3 nanostructures, on the other hand, have a 1D bubble-nanorod shape, with hollow nanospheres surrounded by carbon nanofibers, as seen in TEM images (Figure 4c,d). This one-of-a-kind structure, which is held together by a 3.0 nm shell and carbon matrix, keeps the volume from changing too much during cycling. This lets it keep 84% of its capacity after 300 cycles (Figure 4e). The $Li_{1.2}Ni_{2.5}B_2$ has a 1D shape with Ni/B-based honeycomb channels and tunnel-type structures, which was confirmed by TEM (Figure 4f). The lattice spacing (0.42 nm) and even distribution of elements make it easy for Li^+ to intercalate and diffuse. This leads to good stability over 500 cycles (Figure 4g). Finally, Ge-CNFs-(700) nanofibers have a flat shape with even widths and smooth surfaces, as seen in TEM images (Figure 4h). These features make them good for moving Li^+ and electrons. This design, combined with a carbon coating, delivers ultra-high fast-charging performance, retaining 281.6 mA h g^{-1} after 5000 cycles (Figure 4i). These studies underscore how distinct 1D morphologies—ranging from hexagonal frameworks in $Sr_8Ti_7S_{21}$ to hollow nanospheres in Fe_2O_3, honeycomb channels in $Li_{1.2}Ni_{2.5}B_2$, and smooth nanofibers in Ge-CNFs—dictate their electrochemical behavior, emphasizing the importance of tailored structural design for optimizing energy storage performance.

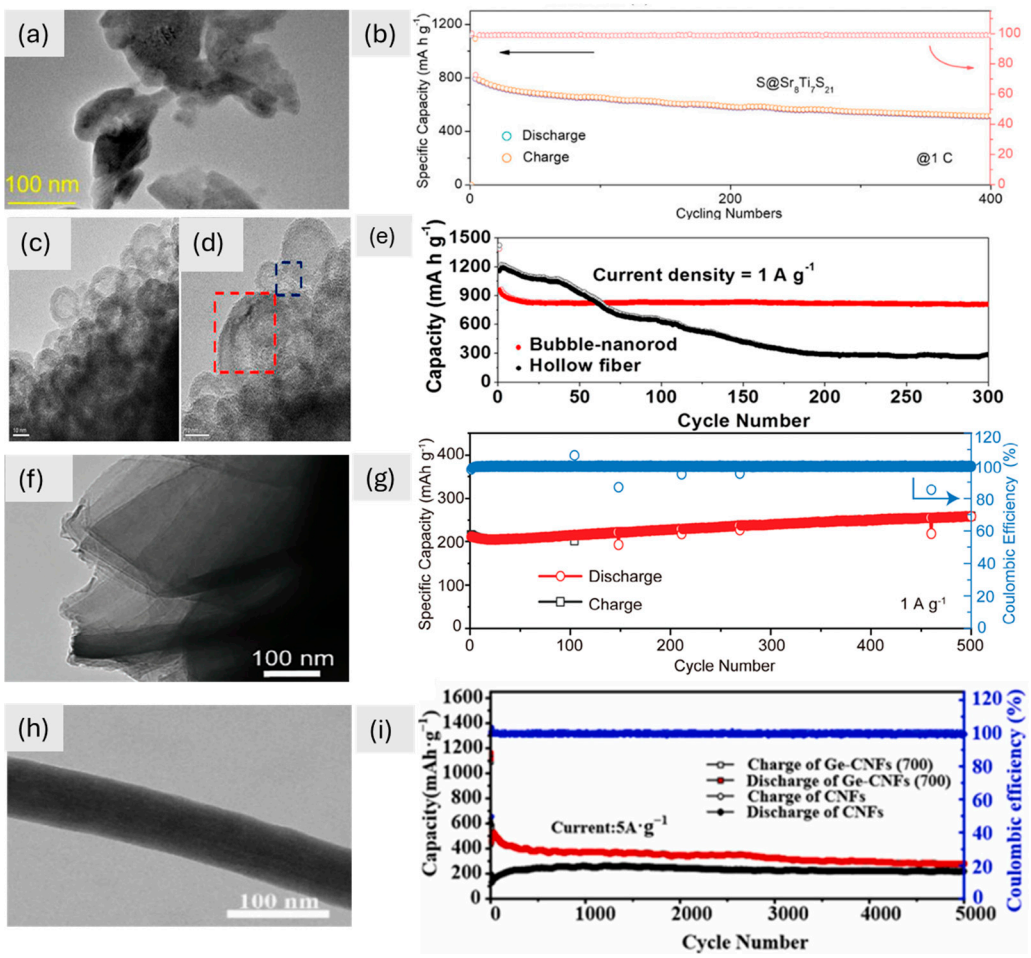

Figure 4. (**a**) TEM image of $Sr_8Ti_7S_{21}$ at 100 nm, (**b**) cycling performances of electrode $S@Sr_8Ti_7S_{21}$ [16]. Copyright © 2024 Wiley. (**c**,**d**) Fe_2O_3/C composite TEM images at 10 nm, (**e**) cyclic performance of different materials at a current density of 1 A g^{-1} [81]. Copyright © 2015, American Chemical Society. (**f**) TEM image of $Li_{1.2}Ni_{2.5}B_2$ at 100 nm, (**g**) cycling performance up to 500 cycles of $Li_{1.2}Ni_{2.5}B_2$ [80]. Copyright © 2024 Wiley. (**h**) TEM image (100 nm) of Ge-CNFs-(700), (**i**) cycling performance up to 5000 cycles of CNFs and Ge-CNFs-(700) [77]. Copyright © 2024, Elsevier.

3.3. Two-Dimensional Inorganic Electrode Materials

The remarkable physical and chemical properties of two-dimensional inorganic materials, such as exfoliated graphene, together with their high surface-to-mass ratio, have sparked significant interest in the field of lithium-ion batteries. Two-dimensional transition metal carbides and nitrides, or MXenes, due to their remarkable structural flexibility and intricate surface chemistry, have garnered significant attention in the field of energy storage.

Among all the 2D materials, several investigations have indicated the potential uses of MXenes in LIBs [138–140]. Many new studies have put into evidence interesting qualities, including strong mechanical properties, variable bandgap energies, large electrochemically active surfaces, and great electrical conductivity. Multilayer MXenes may have a range of inorganic chemicals added to their structure to improve their effective dispersion in aqueous solutions. They are intriguing options for electrode material for LIBs because their layered structure makes it easier to store ions. In fact, Li^+ can intercalate at low voltages (0.2 V to 0.6 V) with little diffusion barriers. It is necessary to assess the reversible potential of LIBs that include MXenes in light of the lowered diffusion barriers. Findings from theoretical studies indicate that MXenes with a smaller number of formula units have a higher reversible capacity and quicker diffusion rates than those with a larger number of formula units. On the other hand, the same relationship holds true in the inverse scenario [139].

For instance, despite having a low diffusion barrier of 0.42 eV, the material $V_4C_3O_2$ exhibits a relatively low capacity of 148 mA h g^{-1} compared to other materials because of faster ion movement but may lead to lower capacity if the material cannot host many ions. On the other side, V_2CO_2 has a far higher diffusion barrier of 0.82 eV than other materials, even though it has a substantially higher capacity value of 276 mA h g^{-1}. Also, the diffusion barrier of Ti_3C_2 is 0.07 eV, which is much lower than that of graphite, which is 0.3 eV. The previously mentioned benefits of MXenes are significant but we still need further study to fully understand their intercalated structures and the mechanisms associated with them [140]. Research on titanium carbide by M. Naguib et al. [141] revealed that Li^+ intercalates inside the material's layers. The study aimed to utilize titanium carbide as an anode material in lithium-ion batteries. Zhang et al. [142] reported highly conductive Ti_3C_2 MXene decorated with Sn^{4+} ions, emphasizing the material's promising application in lithium-ion anodes. Researchers have investigated several MXene materials, including Ti_2CT_x, Nb_2CT_x, $Ti_3C_2T_x$, and V_2CT_x, for their potential use as LIBs. The letter Tx corresponds to the functional surface terminal groups in these materials. Because of its remarkable conductivity and primarily electrochemical behavior, MXene exhibits significant volumetric capacitances. The materials show substantial improvements in gravimetric performance as compared to activated carbon, demonstrating capacitances of around 210 farads per gram at a rate of 10 volts per second [143]. Lukatskaya et al. found that Ti_3C_2 in a microporous configuration reached a value of 300 Fg^{-1} capacitance at a scan rate of 101 mV s^{-1} [143]. This result was exceptional for electrochemical behavior, highlighting the significant potential of MXenes in energy storage applications.

The inorganic 2D materials, aside from transition metal carbides/nitrides (MXenes), that have been stated for use in high-performance LIBs can be categorized into several groups: graphene and the derivatives of graphene, such as graphene oxides, silicene, borophene, stanine, phosphorene, and germanene (called elemental analogs of graphene); 2D structures like hBN, transition metal dichalcogenides (TMDs), and transition metal oxides (TMOs); and newly emerging 2D materials.

Among the reported 2D materials, graphene and its derivatives have undergone the most extensive study. Pure graphene exhibits an exceptionally large surface area of 2630 m^2 g^{-1}, alongside remarkable charge carrier mobility, a thermal conductivity of

5000 W mK^{-1}, and a Young's modulus of 1 TPa [144,145]. Graphite, being the most commonly utilized electrode material for high-energy storage devices, has a theoretical capacity that falls short of meeting the growing demand; it also lacks sufficient rate capability. Derived from graphite, graphene exhibits a larger surface area and increased interlayer spacing compared to graphite, prompting extensive exploration of its potential as an electrode material. The ability of both sides of graphene to adsorb ions suggests that its capacity could potentially be twice that of graphite when utilized as an electrode material. The experimental studies on graphene anodes [146] and graphene cathodes [147] have demonstrated the feasibility of the concept of graphene electrodes.

Shu et al. [148] developed a porous graphene paper as an anode material for LIBs. This material demonstrates a discharge capacity of 400 mA h g^{-1}, even at a high current density of 2000 mA g^{-1}. The electrochemical characteristics of a material also depend upon the synthesis process and techniques used for the testing. Cohn et al. [149] created a nano-manufactured material specifically designed for LIBs. It was a hybrid graphene-single-walled CNT. By testing this material, they calculated the capacity of 2640 mA h g^{-1} at the rate of 0.186 A g^{-1}. In another paper, Hassoun et al. [150] reported a capacity of 165 mA h g^{-1}, which was basically calculated by a graphene-based battery with an energy density of 190 W h kg^{-1}.

Researchers extensively examined graphene-based composites alongside other active materials that may achieve greater capacities. Layered transition metal oxides are very attractive options. They offer the potential for high capacity, exhibit excellent chemical stability, and are cost-effective. Ni et al. [91] developed a composite material of MoO_2 nanosheets with a carbon matrix. MoO_2 presents itself as a noteworthy electrode material, exhibiting moderate discharge and charge voltages. This composite, when utilized as the anode material in high-performance LIBs, has demonstrated a remarkable capacity of 1051 mA h g^{-1} over 100 cycles at a current of 0.5 A g^{-1}. Nb_2O_5 nanosheets have been synthesized through experimental methods and evaluated for their performance as the anode in Li-ion batteries. They achieved a lithium capacity of 184 mA h g^{-1} and demonstrated commendable rate capability at intermediate discharge/charge voltages between 1.0 and 2.5 V [151].

Additionally, 2D transition metal dichalcogenides (TMDs) represent an expanding category of two-dimensional materials. Recently, there has been a big rise in the discovery and production of new 2D TMDs with a wide range of electric properties that can be used as LIB electrode materials.

Xiao et al. [152] developed a composite (MoS_2/PEO), utilizing PEO to stabilize the disordered structure. The PEO/MoS_2 composite demonstrated an impressive capacity of 1000 mA h g^{-1}. Liu et al. [88] synthesized and reported the electrochemical characteristics of the graphene and MoS_2 composite. At the specific current value of 100 mAg^{-1}, the impressive capacity of 1351 mA h g^{-1} was shown by this material after 200 cycles (charging/discharging). Conversely, significant focus has been directed towards the fabrication of SnS_2 and graphene composites, with reported significant capacities up to 1000 mA h g^{-1}. SnS_2 nanosheets represent a notable option for creating composites with graphene [153–155]. Researchers are finding ways and techniques not only to increase the LIBs performance but also the combinations of lithium with other metals, for example, Qu et al. [153] reported on the development of composite material for high-performance lithium/sodium batteries. This SnS_2/rGO combined material shows a capacity of 544 mA h g^{-1} at a rate of 2A g^{-1}. Alongside phosphorene, recent studies have also explored other two-dimensional (2D) monoelemental materials that have a similar lattice structure to graphene, including silicene, germanene, borophene, and stanine [156–160].

Bo et al. created a 2D carbon/Si composite using the ice template technique supported by ultrasonic atomization. They used this composite (NPCN/Si-2) as an electrode material to evaluate its electrochemical characteristics. This material showed a capacity value of 1977 mA h g^{-1} at the rate of 100 mA g^{-1} after 100 cycles (charging/discharging). The material even tested for 1000 charge-discharge cycles and it shows a stable capacity of 889 mA h g^{-1} [13]. Do et al. stated a unique synthesis method for improving the performance of Si-based anode material using the spray drying technique. The material demonstrates the capacity of 1224 mA h g^{-1} and an outstanding retention rate of 82% after the 100 cycles at 20 mA g^{-1} current density; this special combination produces high capacities and robust retention behaviors. They constructed a LIB consisting of silicon-based nanocarbon material as an anode. After 200 cycles, the lithium-ion battery full cell shows 65% capacity retention with an energy density of 350 Wh kg^{-1} [93].

Abdul et al. reported a B_4C_3 monolayer with a storage capacity of 2770 mA hg^{-1}. They conducted theoretical studies using density functional theory to investigate the electrochemical viability of the material. Using the values of the diffusion coefficient and ionic conductivity, they explained the behavior of the material and predicted its potential for use as an anode in lithium-ion batteries [14]. Zaid et al. used a hydrothermal process to make titanium (TiO_2) and C-TiO_2 material, which improved the Li-battery's electrical performance. As an anode material, the composite was a well-established and very effective carbon-doped TiO_2 (C-TiO_2). The findings demonstrated 400 and 500 mA hg^{-1} charge capabilities at 100 mAg^{-1} [161]. Siwei et al. synthesized the Cu_3Si/Si nanowires that displayed an initial 89% coulombic efficiency and a specific capacity of 2630 mA h g^{-1}, after 100 cycles of charging and discharging, resulting in a capacity of 1675 mA h g^{-1} at a current density of 200 mA g^{-1} [15].

The three studies (Figure 5) highlight the significance of 2D morphology in enhancing the electrochemical performance of Si-based materials, as revealed by TEM analysis. The first study demonstrates a 2D crumpled nanosheet morphology in NPCN/Si-2, where Si nanoparticles are uniformly embedded, creating a 3D interconnected network. This structure, confirmed by TEM (Figure 5a,b), ensures efficient Li-ion accessibility, reduces aggregation, and provides structural stability, resulting in high capacity and cycling stability (Figure 5c). In the second study, the 2D structure of the rGO and SWCNT layers creates an interconnected network (Figure 5d,e). This restores the sp^2 carbon network, which makes the electrical conductivity and Li-ion transport better. This results in high capacity and retention (82%) after 100 cycles (Figure 5f). In the third study, Cu_3Si/Si nanowires have a shape that is similar to that of a flat surface. This is because Cu_3Si/Si nanoparticles are mixed in with Si nanowires, making a complex that can grow in size, as seen in the lattice fringes of TEM (Figure 5g). This morphology enhances cycling stability and supports high capacities (Figure 5l). In all cases, the inorganic materials (Si, Cu_3Si) play a critical role in maintaining structural integrity and electrochemical performance while TEM analysis provides detailed insights into the morphological features that directly influence the material's efficiency and stability (Figure 5).

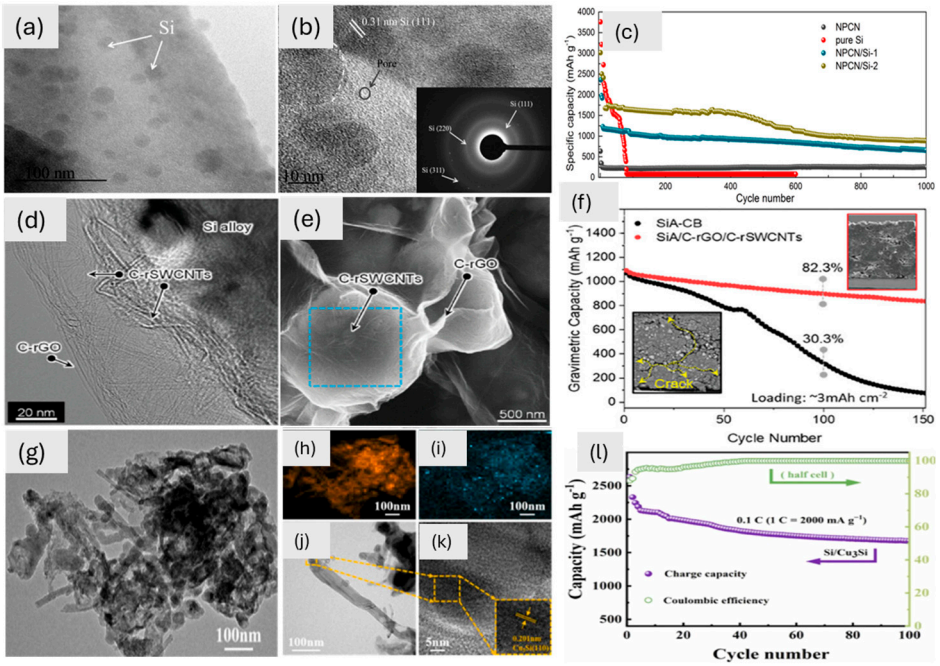

Figure 5. (**a**,**b**) High-resolution TEM images of NPCN/Si-2 with an inset of the SAED pattern and (**c**) electrochemical performance of pure Si, NPCN, and composites at the rate of 1 A g^{-1} [13]. Copyright © 2024 Elsevier. (**d**) TEM image (20 nm) of a SiA/NC, (**e**) SEM image (500 nm) of SiA/NC, (**f**) cyclic performance of materials with the inset showing cross-sectional images after 150 cycles of the materials, SiA and SiA/NC [93]. Copyright © 2023 Wiley. (**g**) TEM image (100 nm) of the produced nanowires, (**h**–**k**) Cu-Si 3:16 EDS map scanning, (**l**) cycle performance of Si/Cu_3Si for 100 cycles at 0.2 A g^{-1} [15]. Copyright © 2024 Elsevier.

3.4. Three-Dimensional Inorganic Electrode Materials

Additionally, 3D materials like SnO_2, Fe_2O_3, TiO_2, V_2O_5, and conducting polymers still face challenges because they have lower energy capacities than 1D and 2D materials [102,103,162,163]. A large-scale study is also being given to the electrochemical characteristics of 3D inorganic perovskite materials for LIBs. The three-dimensional shape of the highly linked crystal structure of the $CsPbCl_3$ perovskite makes it easier for electrons to move and for Li-ions to diffuse. For lithium-ion batteries to operate well over an extended period, this 3D design enhances structural stability and ionic conductivity. Furthermore, the strong $CsPbCl_3$ framework reduces volume expansion, improving cycle stability and capacity retention. $CsPbCl_3$ material with a capacity of 612.3 mA h g^{-1} at a rate of 50 mA g^{-1} was reported by Pal et al. [106]. After 100 cycles, Paul et al. found that the $CsPbBr_3$ material had a reduced capacity of 261 mA h g^{-1} at a current density of 60 mA g^{-1}. When we look at $CsPbBr_3$ with XPS, we can see that its chemical composition is stable (Figure 6c). This means that it will work well during cycling (charging/discharging) [100]. According to Kaisar et al., the $CsPbI_3$ material can sustain performance for up to 100 cycles with a capacity of 235 mA h g^{-1} at 40 mA g^{-1}. It was found that the crystal structures of the $CsPbBr_3$ and $CsPbI_3$ perovskites are orthorhombic by XRD. This is necessary for them to be stable in lithium-ion batteries from an electrochemical point of view. The Rietveld refinement of $CsPbI_3$ shows that the unit cell volume changes during lithiation, affecting how much lithium can be stored (Figure 6b) [101]. According to Liu et al., the $CsPbBr_3$@CNTs composite has an enhanced capacity of 470.2 mA h g^{-1} at 100 mA g^{-1} after 200 charge-discharge cycles. Improved conductivity and stability are shown by the $CsPbBr_3$@CNTs composite's ability to retain its structure (Figure 6a) [99]. The stability and lithium storage potential of 3D perovskites in energy storage applications are highlighted by these structural insights. Wu et al. found that the promising electrode material $Cs_2NaBiCl_6$

has the highest capacity at 775 mA h g^{-1} when the current density is 75 mA g^{-1} for 25 cycles [105]. Another material, $Cs_2NaErCl_6$, was described by Yang et al. in a different paper. It has a capacity of 120 mA hg^{-1} at a high current density of 300 mA g^{-1} after 500 cycles [98].

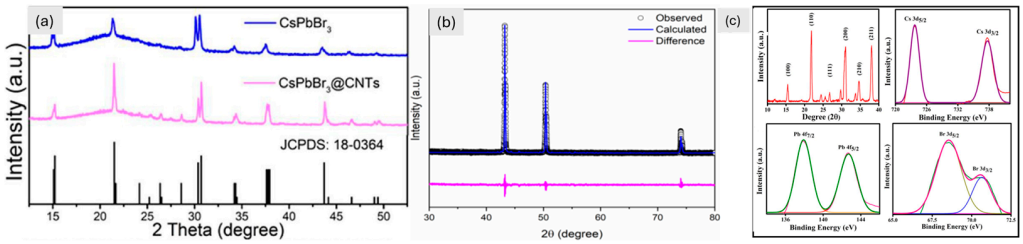

Figure 6. (**a**) XRD of $CsPbBr_3$ and composite [99], Copyright © 2021 Elsevier, (**b**) showing the XRD pattern of CsPbI3 after 100 charge-discharge cycles [101], Copyright © 2021 MDPI. (**c**) $CsPbBr_3$ XRD pattern and XPS spectra of Cs/Pb/Br_3 separately [100], Copyright © 2021, American Chemical Society.

At the moment, 3D-ordered porous (3DOP) electrode materials are being intensively recognized and investigated for their potential use in high-performance electrochemical energy storage systems. One of the advantages of 3DOP electrodes is that they have a periodic structure. This structure enables the connecting walls to reach into the unoccupied pores, which prevents the walls from being pulverized. These materials provide a high surface area along with interconnected pores, which enhance the efficiency of ion transport and electron pathways. The distinctive architecture boosts the charge and discharge rates as well as overall energy density. Furthermore, 3DOP materials demonstrate remarkable mechanical stability, accommodating volume fluctuations during cycling to enhance battery longevity [97].

Titanium dioxide (TiO_2) has undergone a significant examination for use in high-performance LIBs. TiO_2 is chemically stable, abundant in nature, very cost-effective, and environmentally friendly element. In most cases, it is used as an anode material for Li storage. It has been shown that the rutile TiO_2 electrode has an early discharge capacity of 608 mA h g^{-1}. This is a lot more than the theoretical capacity of TiO_2, which is 168 mA h g^{-1} for $Li_{0.5}TiO_2$ and 336 mA h g^{-1} for $LiTiO_2$. Furthermore, this 3DOP rutile TiO_2 electrode demonstrates remarkable performance, reaching up to 5000 cycles without the use of any binders [97]. Transition cobalt oxides are also important materials for use in high-performance LIBs with impressive theoretical capacities. In the case of Co_3O_4, the theoretical value of 890 mA h g^{-1} capacity is reported. And in the case of CoO, the theoretical value of 716 mA h g^{-1} capacity is reported [164–166]. It is not possible to use CoO in LIBs as an anode material in experiments because it loses a lot of its capacity after long cycles, which is caused by big changes in volume. In addressing this issue, three-dimensional ordered porous carbon inverse opals have been employed to encapsulate CoO nanoparticles [104]. After 1000 cycles, the CoO/C electrode exhibits a notable value of 674 mA h g^{-1} capacity, which is 94% of the theoretical capacity. For active nanoparticles, the three-dimensional ordered porous carbon structure serves both a dimensional limitation and an interpenetrated, continuous conducting network.

On the other hand, iron oxides stand out among the numerous transition metal oxides as a widely examined anode material due to their numerous advantages. These include impressive theoretical capacities as well as their abundant availability and environmentally friendly properties. For example, Fe_3O_4 has a reported capacity value of 926 mA h g^{-1} whereas Fe_2O_3 has a reported capacity value of 1007 mA h g^{-1}. In another publication, the capacities of 3DOP α-Fe_2O_3 are reported as 1883 (discharge) and 1139 mA h g^{-1} (charge), respectively [167].

Among all the many types of anode materials, investigations that compare Si anodes have shown that they have the greatest specific capacity of any of the other possibilities. As the need for energy storage solutions that work well and last a long time grows, studying bulk-silicon- and nano-silicon-based anodes in lithium-ion secondary cells looks like a good idea. That is the reason they have been studied on a large scale. It is thought that both bulk-silicon and nano-silicon (Si)-based anodes for lithium-ion secondary cells could be used to store energy in the future and they have a high theoretical capacity (about 4200 mA h g^{-1}) [168]. One of the most notable drawbacks, however, is the large volume expansion of this material (about 400%) that takes place during the electrochemical processes with Li ions. This significantly restricts the practical use of these materials [169,170]. There are several Si anode composites with Ni (Si/Ni) that were manufactured using the method of electrodeposition in order to solve the pulverization problem [171,172].

Additional electrochemically active anode materials, including graphene [173], $TiNb_2O_7$ [174], MoS_2 [175], and Ge [176,177], were also developed as 3DOP electrodes for Li-ion storage.

SEM and TEM confirm the 3D-ordered macroporous (3DOM) structure of $TiNbO_7$, which displays well-organized "honeycomb" pores with linked macropores (~100 nm diameter) and inorganic walls (~50 nm thick) (Figure 7). It makes it easier for lithium ions to move around and keeps the structure stable during cycling. This very porous three-dimensional framework is better at storing lithium ions. Because it is linked in three dimensions, this 3DOM-$TiNbO_7$ is a good material for the anode of high-performance lithium-ion batteries [174]. Also, tin dioxide is one of the examined anode materials for LIBs, with an irreversible conversion reaction alongside a reversible alloying reaction, (SnO_2/Sn + Li_2O) and (Sn/$Li_{4.4}Sn$), respectively [178–180]. The investigation of commercial inorganic cathode nanomaterials for LIBs primarily centers on $LiFePO_4$. The olivine-structured $LiFePO_4$ is a highly favorable alternative to $LiCoO_2$ due to its environmentally friendly nature. The primary drawback lies in its inadequate conductivity and rate capability [181]. To solve the problem of low conductivity, some conductive material can be used as a mixture with $LiFePO_4$ electrodes. $LiMnO_2$ has garnered significant attention thanks to its impressive theoretical capacity near 300 mA h g^{-1} along with good experimental capacities [182]. The $LiMnO_2$ crystal has both a layered monoclinic structure and an orthorhombic structure. The zigzag arrangement of Li and Mn ions highlights the orthorhombic structure.

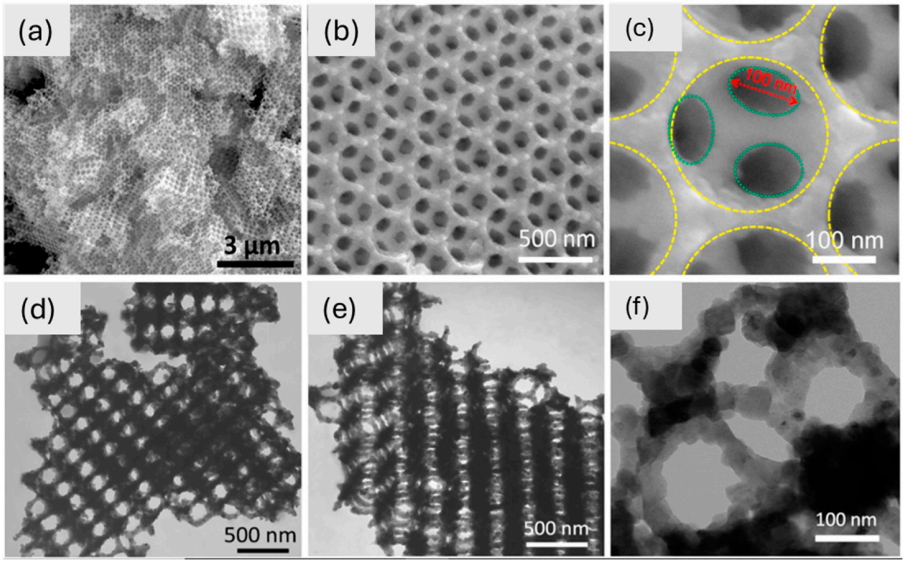

Figure 7. (**a**–**c**) SEM images of $TiNb_2O_7$ at different magnifications and (**d**–**f**) TEM images of $TiNb_2O_7$ at different magnifications [174]. Copyright © 2017 Elsevier.

Although 3D materials have several benefits, poor cycle life; scaling issues; and expensive, complicated production restrict their use in high-performance LIBs. They are less appropriate for traditional usage since they often increase power density while decreasing volumetric energy density. Efficiency and longevity may be impacted by side reactions and unequal electrolyte penetration brought on by large surface areas. It is challenging to compete with cost-effective, optimized materials like graphite. Three-dimensional materials still have challenges with cost, performance, and scalability, despite continuous research aimed at enhancing their capabilities.

4. Conclusions and Future Outlook

Extensive efforts have been invested to develop novel and efficient electrode materials for high-performance energy storage devices based on inorganic oxides. However, the devices made up of these electrodes are characterized by lower energy and power density [183,184]. This study reveals that the electrode material properties like surface areas, charge storage sites, chemical reactions, unique bonding, and interactions with the electrolyte play a crucial role in defining the electrochemical performances of electrodes used in lithium-ion batteries.

LIBs can utilize zero-dimensional nanoparticles, such as quantum dots, and three-dimensional structures like graphene multilayers; however, these nanostructures are less prevalent compared to one- and two-dimensional alternatives [185–190]. One-dimensional nanoparticles, such as nanowires and nanotubes, show high conductivity and ability to improve charge transfer. Graphene and other layered materials exhibit exceptional electrical conductivity and a large surface area, both of which are essential for effective energy storage. Each type of nanostructure addresses specific performance metrics for LIBs. The most promising silicon-based architectures for high energy density are 0D and 1D structures. Additionally, 1D CNTs and 2D graphene provide a better rate performance for rapid charge/discharge. MXenes and 3D hierarchical structures are particularly noteworthy for long-term cycle stability.

This study allows us to highlight that optimizing the morphology of nanomaterials significantly enhances the electrochemical performance of LIB electrodes. To obtain high energy density, fast charge/discharge rates, and long-term stability, future research should focus on scalable ways to make hybrid structures that combine 0D, 1D, 2D, and 3D materials. A hybrid method that combines many nanostructures (for example, 3D frameworks with built-in 0D or 2D materials) could improve battery performance. This would bridge the gap between lab-based innovation and commercial scalability. Furthermore, investigating innovative surface alterations and electrolyte interactions may enhance economic viability even further.

Author Contributions: Conceptualization, M.H.K. and V.T.; methodology M.H.K. and V.T.: investigation, M.H.K. resources, P.L. and V.T.; data curation, M.H.K.; writing—original draft preparation, M.H.K.; writing—review and editing, M.H.K., P.L. and V.T.; supervision, V.T.; funding acquisition, P.L. and V.T. All authors have read and agreed to the published version of the manuscript.

Funding: The development of this work is framed in the Environmentally Friendly Aviation for All Classes of Aircraft (EFACA) project. This project is funded by the European Union Horizon Europe research and innovation programme (HORIZON-CL5-2021-D5-01-05) under grant agreement no. 101056866.

Data Availability Statement: No new data were created or analyzed in this study. Data sharing is not applicable to this article.

Acknowledgments: MHK acknowledges the support by the Dottorato di Ricerca Nazionale in Photovoltaics funded by Italian University Ministry.

Conflicts of Interest: The authors declare no conflicts of interest. The funders had no role in the design of this study; in the collection, analyses, or interpretation of data; in the writing of the manuscript; or in the decision to publish the results.

References

1. Zhang, K.; Han, X.; Hu, Z.; Zhang, X.; Tao, Z.; Chen, J. Nanostructured Mn-based oxides for electrochemical energy storage and conversion. *Chem. Soc. Rev.* **2015**, *44*, 699–728. [CrossRef] [PubMed]
2. Goodenough, J.B. Evolution of strategies for modern rechargeable batteries. *ACC Chem. Res.* **2013**, *46*, 1053–1061. [CrossRef] [PubMed]
3. Dunn, B.; Kamath, H.; Tarascon, J.-M. Electrical Energy Storage for the Grid: A Battery of Choices System power ratings, module size. *Science* **2011**, *334*, 928–935. [CrossRef] [PubMed]
4. Chodankar, N.R.; Dubal, D.P.; Kwon, Y.; Kim, D.H. Direct growth of $FeCo_2O_4$ nanowire arrays on flexible stainless steel mesh for high-performance asymmetric supercapacitor. *NPG Asia Mater.* **2017**, *9*, e419. [CrossRef]
5. Wang, F.; Wu, X.; Li, C.; Zhu, Y.; Fu, L.; Wu, Y.; Liu, X. Nanostructured positive electrode materials for post-lithium ion batteries. *Energy Environ. Sci.* **2016**, *9*, 3570–3611. [CrossRef]
6. Wang, F.; Wang, X.; Chang, Z.; Zhu, Y.; Fu, L.; Liu, X.; Wu, Y. Electrode materials with tailored facets for electrochemical energy storage. *Nanoscale Horiz.* **2016**, *1*, 272–289. [CrossRef]
7. Wang, F.; Wu, X.; Yuan, X.; Liu, Z.; Zhang, Y.; Fu, L.; Zhu, Y.; Zhou, Q.; Wu, Y.; Huang, W. Latest advances in supercapacitors: From new electrode materials to novel device designs. *Chem. Soc. Rev.* **2017**, *46*, 6816–6854. [CrossRef]
8. Liu, J.; Li, N.; Goodman, M.D.; Zhang, H.G.; Epstein, E.S.; Huang, B.; Pan, Z.; Kim, J.; Choi, J.H.; Huang, X. Mechanically and chemically robust sandwich-structured C@Si@C nanotube array Li-ion battery anodes. *ACS Nano* **2015**, *9*, 1985–1994. [CrossRef] [PubMed]
9. Wang, C.; Jiang, C.; Xu, Y.; Liang, L.; Zhou, M.; Jiang, J.; Singh, S.; Zhao, H.; Schober, A.; Lei, Y. Article type: Communication A selectively permeable membrane for enhancing cyclability of organic sodium-ion batteries. *Adv. Mater.* **2016**, *28*, 9182–9187. [CrossRef] [PubMed]
10. Sun, H.; Mei, L.; Liang, J.; Zhao, Z.; Lee, C.; Fei, H.; Ding, M.; Lau, J.; Li, M.; Wang, C.; et al. Three-dimensional holey-graphene/niobia composite architectures for ultrahigh-rate energy storage. *Science* **2017**, *356*, 599–604. [CrossRef]
11. Sun, Y.; Liu, N.; Cui, Y. *Promises and Challenges of Nanomaterials for Lithium-Based Rechargeable Batteries*; Nature Publishing Group: London, UK, 2016. [CrossRef]
12. Bruce, P.G.; Freunberger, S.A.; Hardwick, L.J.; Tarascon, J.M. *LiO_2 and LigS Batteries with High Energy Storage*; Nature Publishing Group: London, UK, 2012. [CrossRef]
13. Liang, B.; Tan, W.; Chen, M.; Yi, M.; Hu, J.; Zeng, K.; Wang, Y.; Li, Y.; Yang, G. Facile synthesis of two-dimensional carbon/Si composite assembled by ultrasonic atomization-assisted-ice template technology as electrode for lithium-ion battery. *J. Alloys Compd.* **2024**, *976*, 173030. [CrossRef]
14. Majid, A.; Najam, U.; Ahmad, S.; Alkhedher, M. On the prospects of using B_4C_3 as a potential electrode material for lithium-ion batteries. *Mater. Sci. Semicond. Process* **2024**, *176*, 108320. [CrossRef]
15. Jiang, S.; Cheng, J.; Nayaka, G.P.; Dong, P.; Zhang, Y.; Xing, Y.; Zhang, X.; Du, N.; Zhou, Z. Efficient electrochemical synthesis of Cu_3Si/Si hybrids as negative electrode material for lithium-ion battery. *J. Alloys Compd.* **2024**, *998*, 174996. [CrossRef]
16. Yang, D.; Han, Y.; Li, M.; Li, C.; Bi, W.; Gong, Q.; Zhang, J.; Zhang, J.; Zhou, Y.; Gao, H.; et al. Highly Conductive Quasi-1D Hexagonal Chalcogenide Perovskite Sr_8 Ti_7 S_{21} with Efficient Polysulfide Regulation in Lithium-Sulfur Batteries. *Adv. Funct. Mater.* **2024**, *34*, 2401577. [CrossRef]
17. Wei, Q.; Xiong, F.; Tan, S.; Huang, L.; Lan, E.H.; Dunn, B.; Mai, L. *Porous One-Dimensional Nanomaterials: Design, Fabrication and Applications in Electrochemical Energy Storage*; Wiley-VCH Verlag: Weinheim, Germany, 2017. [CrossRef]
18. Liu, Z.; Yuan, X.; Zhang, S.; Wang, J.; Huang, Q.; Yu, N.; Zhu, Y.; Fu, L.; Wang, F.; Chen, Y.; et al. *Three-Dimensional Ordered Porous Electrode Materials for Electrochemical Energy Storage*; Nature Publishing Group: London, UK, 2019. [CrossRef]
19. Cui, G.; Gu, L.; Thomas, A.; Fu, L.; van Aken, P.A.; Antonietti, M.; Maier, J. A Carbon/Titanium Vanadium Nitride Composite for Lithium Storage. *ChemPhysChem* **2010**, *11*, 3219–3223. [CrossRef]
20. Lee, K.T.; Lytle, J.C.; Ergang, N.S.; Oh, S.M.; Stein, A. Synthesis and rate performance of monolithic macroporous carbon electrodes for lithium-ion secondary batteries. *Adv. Funct. Mater.* **2005**, *15*, 547–556. [CrossRef]
21. Che, G.; Lakshmi, B.B.; Fisher, E.R.; Martin, C.R. Carbon nanotubule membranes for electrochemical energy storage and production. *Nature* **1998**, *393*, 346–349. [CrossRef]
22. Guo, B.; Wang, X.; Fulvio, P.F.; Chi, M.; Mahurin, S.M.; Sun, X.-G.; Dai, S. Soft-templated mesoporous carbon-carbon nanotube composites for high performance lithium-ion batteries. *Adv. Mater.* **2011**, *23*, 4661–4666. [CrossRef]

23. Li, S.; Luo, Y.; Lv, W.; Yu, W.; Wu, S.; Hou, P.; Yang, Q.; Meng, Q.; Liu, C.; Cheng, H.-M. Vertically aligned carbon nanotubes grown on graphene paper as electrodes in lithium-ion batteries and dye-sensitized solar cells. *Adv. Energy Mater.* **2011**, *1*, 486–490. [CrossRef]
24. Chen, J.; Xu, L.; Li, W.; Gou, X. α-Fe_2O_3 nanotubes in gas sensor and lithium-ion battery applications. *Adv. Mater.* **2005**, *17*, 582–586. [CrossRef]
25. Taberna, P.L.; Mitra, S.; Poizot, P.; Simon, P.; Tarascon, J.M. *High Rate Capabilities Fe_3O_4-Based Cu Nano-Architectured Electrodes for Lithium-Ion Battery Applications*; Nature Publishing Group: London, UK, 2006. [CrossRef]
26. Kim, W.T.; Jeong, Y.U.; Lee, Y.J.; Kim, Y.J.; Song, J.H. Synthesis and lithium intercalation properties of Li_3VO_4 as a new anode material for secondary lithium batteries. *J. Power Sources* **2013**, *244*, 557–560. [CrossRef]
27. Dong, S.; Chen, X.; Zhang, X.; Cui, G. Nanostructured transition metal nitrides for energy storage and fuel cells. *Coord. Chem. Rev.* **2013**, *257*, 1946–1956. [CrossRef]
28. Serhan, M.; Jackemeyer, D.; Long, M.; Sprowls, M.; Diez Perez, I.; Maret, W.; Chen, F.; Tao, N.; Forzani, E. Total iron measurement in human serum with a smartphone. In *AIChE Annual Meeting, Conference Proceedings*; American Institute of Chemical Engineers: New York, NY, USA, 2019.
29. Lee, J.T.; Zhao, Y.; Thieme, S.; Kim, H.; Oschatz, M.; Borchardt, L.; Magasinski, A.; Cho, W.-I.; Kaskel, S.; Yushin, G. Sulfur-infiltrated micro-and mesoporous silicon carbide-derived carbon cathode for high-performance lithium sulfur batteries. *Adv. Mater.* **2013**, *25*, 4573–4579. [CrossRef]
30. Naguib, M.; Halim, J.; Lu, J.; Cook, K.M.; Hultman, L.; Gogotsi, Y.; Barsoum, M.W. New two-dimensional niobium and vanadium carbides as promising materials for li-ion batteries. *J. Am. Chem. Soc.* **2013**, *135*, 15966–15969. [CrossRef] [PubMed]
31. Seng, K.H.; Park, M.H.; Guo, Z.P.; Liu, H.K.; Cho, J. Catalytic role of ge in highly reversible GeO_2/Ge/C nanocomposite anode material for lithium batteries. *Nano Lett.* **2013**, *13*, 1230–1236. [CrossRef] [PubMed]
32. Ji, L.; Lin, Z.; Alcoutlabi, M.; Zhang, X. Recent developments in nanostructured anode materials for rechargeable lithium-ion batteries. *Energy Environ. Sci.* **2011**, *4*, 2682–2699. [CrossRef]
33. Luo, S.; Wang, K.; Wang, J.; Jiang, K.; Li, Q.; Fan, S. Binder-free $LiCoO_2$/carbon nanotube cathodes for high-performance lithium ion batteries. *Adv. Mater.* **2012**, *24*, 2294–2298. [CrossRef] [PubMed]
34. Chen, S.; Cao, F.; Liu, F.; Xiang, Q.; Feng, X.; Liu, L.; Qiu, G. Facile hydrothermal synthesis and electrochemical properties of orthorhombic $LiMnO_2$ cathode materials for rechargeable lithium batteries. *RSC Adv.* **2014**, *4*, 13693–13703. [CrossRef]
35. Kobayashi, G.; Yamada, A.; Nishimura, S.-I.; Kanno, R.; Kobayashi, Y.; Seki, S.; Ohno, Y.; Miyashiro, H. Shift of redox potential and kinetics in Lix(MnyFe1-y)PO_4. *J. Power Sources* **2009**, *189*, 397–401. [CrossRef]
36. Hecht, D.S.; Hu, L.; Irvin, G. Emerging transparent electrodes based on thin films of carbon nanotubes, graphene, and metallic nanostructures. *Adv. Mater.* **2011**, *23*, 1482–1513. [CrossRef] [PubMed]
37. Kim, Y.K.; Min, D.H. Durable large-area thin films of graphene/carbon nanotube double layers as a transparent electrode. *Langmuir* **2009**, *25*, 11302–11306. [CrossRef] [PubMed]
38. Yu, M.; Zeng, Y.; Zhang, C.; Lu, X.; Zeng, C.; Yao, C.; Yang, Y.; Tong, Y. Titanium dioxide@polypyrrole core-shell nanowires for all solid-state flexible supercapacitors. *Nanoscale* **2013**, *5*, 10806–10810. [CrossRef]
39. Yu, M.; Zhai, T.; Lu, X.; Chen, X.; Xie, S.; Li, W.; Liang, C.; Zhao, W.; Zhang, L.; Tong, Y. Manganese dioxide nanorod arrays on carbon fabric for flexible solid-state supercapacitors. *J. Power Sources* **2013**, *239*, 64–71. [CrossRef]
40. Tang, Z.; Tang, C.H.; Gong, H. A high energy density asymmetric supercapacitor from nano-architectured $Ni(OH)_2$/Carbon nanotube electrodes. *Adv. Funct. Mater.* **2012**, *22*, 1272–1278. [CrossRef]
41. Yuan, L.; Lu, X.-H.; Xiao, X.; Zhai, T.; Dai, J.; Zhang, F.; Hu, B.; Wang, X.; Gong, L.; Chen, J.; et al. Flexible solid-state supercapacitors based on carbon nanoparticles/MnO_2 nanorods hybrid structure. *ACS Nano* **2012**, *6*, 656–661. [CrossRef]
42. Lu, X.; Zhai, T.; Zhang, X.; Shen, Y.; Yuan, L.; Hu, B.; Gong, L.; Chen, J.; Gao, Y.; Zhou, J.; et al. WO_3-x@Au@MnO_2 core-shell nanowires on carbon fabric for high-performance flexible supercapacitors. *Adv. Mater.* **2012**, *24*, 938–944. [CrossRef]
43. Balogun, M.-S.; Qiu, W.; Wang, W.; Fang, P.; Lu, X.; Tong, Y. Recent Advances in Metal Nitrides as High-Performance Electrode Materials for Energy Storage Devices. *J. Mater. Chem. A* **2015**, *3*, 1364–1387. [CrossRef]
44. Li, Y.; Levine, A.M.; Zhang, J.; Lee, R.J.; Naskar, A.K.; Dai, S.; Paranthaman, M.P. Carbon/tin oxide composite electrodes for improved lithium-ion batteries. *J. Appl. Electrochem.* **2018**, *48*, 811–817. [CrossRef]
45. Yi, H.; Huang, Y.; Sha, Z.; Zhu, X.; Xia, Q.; Xia, H. Facile synthesis of Mo_2N quantum dots embedded N-doped carbon nanosheets composite as advanced anode materials for lithium-ion batteries. *Mater. Lett.* **2020**, *276*, 128205. [CrossRef]
46. Zhang, C.; Li, Y.; Liu, X.; Zheng, X.; Zhao, Y.; Zhang, D. Facile synthesis of $Fe_{24}N_{10}$/porous carbon as a novel high-performance anode material for lithium-ion batteries. *Mater. Lett.* **2021**, *300*, 130196. [CrossRef]
47. Long, B.; Balogun, M.-S.; Luo, L.; Luo, Y.; Qiu, W.; Song, S.; Zhang, L.; Tong, Y. Encapsulated Vanadium-Based Hybrids in Amorphous N-Doped Carbon Matrix as Anode Materials for Lithium-Ion Batteries. *Small* **2017**, *13*, 1702081. [CrossRef]

48. Li, Y.; Wang, X.; Wang, L.; Jia, D.; Yang, Y.; Liu, X.; Sun, M.; Zhao, Z.; Qiu, J. Ni@Ni_3 N Embedded on Three-Dimensional Carbon Nanosheets for High-Performance Lithium/Sodium–Sulfur Batteries. *ACS Appl. Mater. Interfaces* **2021**, *13*, 48536–48545. [CrossRef]
49. Ma, C.; Jia, X.; Liu, X.; Wang, J.; Qiao, W.; Yu, J.; Ling, L. Ultrafine NbN nanoparticle decorated nitrogen-doped carbon nanosheets with efficient polysulfide catalytic conversion for superior Li–S batteries. *J. Power Sources* **2022**, *520*, 230764. [CrossRef]
50. Tarascon, J.-M.; Armand, M. Issues and challenges facing rechargeable lithium batteries. *Nature* **2001**, *414*, 359–367. [CrossRef] [PubMed]
51. Wang, X.; Ding, Y.L.; Deng, Y.P.; Chen, Z. *Ni-Rich/Co-Poor Layered Cathode for Automotive Li-Ion Batteries: Promises and Challenges*; Wiley-VCH Verlag: Weinheim, Germany, 2020. [CrossRef]
52. Xiao, J.; Huang, Y.; Ma, Y.; Li, C.; Fu, L.; Zeng, W.; Wang, X.; Li, X.; Wang, M.; Guo, B. Organic active materials in rechargeable batteries: Recent advances and prospects. *Energy Storage Mater.* **2023**, *63*, 103046. [CrossRef]
53. Jiang, B.; Su, Y.; Liu, R.; Sun, Z.; Wu, D. Calcium Based All-Organic Dual-Ion Batteries with Stable Low Temperature Operability. *Small* **2022**, *18*, 2200049. [CrossRef] [PubMed]
54. Wu, C.; Lu, X.; Peng, L.; Xu, K.; Peng, X.; Huang, J.; Yu, G.; Xie, Y. Two-dimensional vanadyl phosphate ultrathin nanosheets for high energy density and flexible pseudocapacitors. *Nat. Commun.* **2013**, *4*, 2431. [CrossRef]
55. Zhang, K.; Hu, Z.; Tao, Z.; Chen, J. Inorganic &organic materials for rechargeable Li batteries with multi-electron reaction. *Sci. China Mater.* **2014**, *57*, 42–58. [CrossRef]
56. Wu, H.; Cui, Y. Designing nanostructured Si anodes for high energy lithium ion batteries. *Nano Today* **2012**, *7*, 414–429. [CrossRef]
57. Xu, X.; Cao, R.; Jeong, S.; Cho, J. Spindle-like mesoporous α-Fe_2O_3 anode material prepared from MOF template for high-rate lithium batteries. *Nano Lett.* **2012**, *12*, 4988–4991. [CrossRef] [PubMed]
58. Sun, Y.; Hu, X.; Luo, W.; Xia, F.; Huang, Y. Reconstruction of conformal nanoscale MnO on graphene as a high-capacity and long-life anode material for lithium ion batteries. *Adv. Funct. Mater.* **2013**, *23*, 2436–2444. [CrossRef]
59. Gong, Z.; Yang, Y. Recent advances in the research of polyanion-type cathode materials for Li-ion batteries. *Energy Environ. Sci.* **2011**, *4*, 3223–3242. [CrossRef]
60. Mishra, A.; Mehta, A.; Basu, S.; Malode, S.J.; Shetti, N.P.; Shukla, S.S.; Nadagouda, M.N.; Aminabhavi, T.M. Electrode materials for lithium-ion batteries. *Mater. Sci. Energy Technol.* **2018**, *1*, 182–187. [CrossRef]
61. Sharma, Y.; Sharma, N.; Rao, G.V.S.; Chowdari, B.V.R. Nanophase $ZnCo_2O_4$ as a high performance anode material for Li-ion batteries. *Adv. Funct. Mater.* **2007**, *17*, 2855–2861. [CrossRef]
62. Hu, Y.S.; Kienle, L.; Guo, Y.G.; Maier, J. High lithium electroactivity of nanometer-sized rutile TiO_2. *Adv. Mater.* **2006**, *18*, 1421–1426. [CrossRef]
63. Kim, M.G.; Lee, S.; Cho, J. Highly Reversible Li-Ion Intercalating MoP_2 Nanoparticle Cluster Anode for Lithium Rechargeable Batteries. *J. Electrochem. Soc.* **2009**, *156*, A89. [CrossRef]
64. Tiwari, J.N.; Tiwari, R.N.; Kim, K.S. Zero-dimensional, one-dimensional, two-dimensional and three-dimensional nanostructured materials for advanced electrochemical energy devices. *Prog. Mater. Sci.* **2012**, *57*, 724–803. [CrossRef]
65. Ezema, F.I.; Lokhande, C.D.; Lokhande, A.C. *Chemically Deposited Metal Chalcogenide-Based Carbon Composites for Versatile Applications*; Springer International Publishing: Heidelberg, Germany, 2023; ISBN 978-3-03-123400-2. [CrossRef]
66. Yu, W.-J.; He, W.; Wang, C.; Liu, F.; Zhu, L.; Tian, Q.; Tong, H.; Guo, X. Confinement of TiO_2 quantum dots in graphene nanoribbons for high-performance lithium and sodium ion batteries. *J. Alloys Compd.* **2022**, *898*, 162856. [CrossRef]
67. Yin, X.; Zhi, C.; Sun, W.; Lv, L.-P.; Wang, Y. Multilayer NiO@Co_3O_4 @graphene quantum dots hollow spheres for high-performance lithium-ion batteries and supercapacitors. *J. Mater. Chem. A Mater.* **2019**, *7*, 7800–7814. [CrossRef]
68. Li, X.; Meng, X.; Liu, J.; Geng, D.; Zhang, Y.; Norouzi Banis, M.; Li, Y.; Yang, J.; Li, R.; Sun, X.; et al. Tin oxide with controlled morphology and crystallinity by atomic layer deposition onto graphene nanosheets for enhanced lithium storage. *Adv. Funct. Mater.* **2012**, *22*, 1647–1654. [CrossRef]
69. Wang, L.; Shi, Z.; Feng, X.; Zhang, Y.; Cao, S.; Zhang, J. Engineering the micro/nano structure of $Ca_3Co_4O_9$ anode material for lithium-ion batteries. *J. Mater. Sci. Mater. Electron.* **2024**, *35*, 17. [CrossRef]
70. Choi, Y.-H.; Park, H.; Lee, S.; Jeong, H.-D. Synthesis and Electrochemical Performance of π-Conjugated Molecule Bridged Silicon Quantum Dot Cluster as Anode Material for Lithium-Ion Batteries. *ACS Omega* **2020**, *5*, 8629–8637. [CrossRef] [PubMed]
71. Wang, D.; Li, X.; Wang, J.; Yang, J.; Geng, D.; Li, R.; Cai, M.; Sham, T.-K.; Sun, X. Defect-rich crystalline SnO_2 immobilized on graphene nanosheets with enhanced cycle performance for li ion batteries. *J. Phys. Chem. C* **2012**, *116*, 22149–22156. [CrossRef]
72. Zhang, G.; Hou, S.; Zhang, H.; Zeng, W.; Yan, F.; Li, C.C.; Duan, H. High-performance and ultra-stable lithium-ion batteries based on MOF-derived ZnO@ZnO quantum dots/C core-shell nanorod arrays on a carbon cloth anode. *Adv. Mater.* **2015**, *27*, 2400–2405. [CrossRef] [PubMed]
73. Kim, H.; Kim, S.-W.; Park, Y.-U.; Gwon, H.; Seo, D.-H.; Kim, Y.; Kang, K. SnO_2/graphene composite with high lithium storage capability for lithium rechargeable batteries. *Nano Res.* **2010**, *3*, 813–821. [CrossRef]

74. Rana, M.; Boaretto, N.; Mikhalchan, A.; Santos, M.V.; Marcilla, R.; Vilatela, J.J. Composite Fabrics of Conformal MoS2Grown on CNT Fibers: Tough Battery Anodes without Metals or Binders. *ACS Appl. Energy Mater.* **2021**, *4*, 5668–5676. [CrossRef]
75. Paek, S.M.; Yoo, E.J.; Honma, I. Enhanced cyclic performance and lithium storage capacity of SnO_2/graphene nanoporous electrodes with three-dimensionally delaminated flexible structure. *Nano Lett.* **2009**, *9*, 72–75. [CrossRef] [PubMed]
76. Zhou, G.; Wang, D.-W.; Li, F.; Zhang, L.; Li, N.; Wu, Z.-S.; Wen, L.; Lu, G.Q.; Cheng, H.-M. Graphene-wrapped Fe_3O_4 anode material with improved reversible capacity and cyclic stability for lithium ion batteries. *Chem. Mater.* **2010**, *22*, 5306–5313. [CrossRef]
77. Zhang, T.; Huang, T.-T.; Li, X.-J.; Wang, K.; Wang, L.-Y.; Liang, J.-F.; Song, Y.-X.; Li, P.-Y.; Zhang, Y.-G.; Zhang, Y.-H.; et al. Ultra-high rapid-charging performance of 1D germanium anode materials for lithium-ion batteries. *J. Alloys Compd.* **2024**, *976*, 173287. [CrossRef]
78. Pinilla, S.; Park, S.-H.; Fontanez, K.; Márquez, F.; Nicolosi, V.; Morant, C. 0D-1D Hybrid Silicon Nanocomposite as Lithium-Ion Batteries Anodes. *Nanomaterials* **2020**, *10*, 515. [CrossRef]
79. Zhang, L.; Zhang, Y.; Xu, S.; Zhang, C.; Hou, L.; Yuan, C. Scalable Synthesis of One-Dimensional Mesoporous $ZnMnO_3$ Nanorods with Ultra-Stable and High Rate Capability for Efficient Lithium Storage. *Chem. A Eur. J.* **2019**, *25*, 16683–16691. [CrossRef] [PubMed]
80. Liu, W.; Zong, K.; Ghani, U.; Saad, A.; Liu, D.; Deng, Y.; Raza, W.; Li, Y.; Hussain, A.; Ye, P.; et al. Ternary Lithium Nickel Boride with 1D Rapid-Ion-Diffusion Channels as an Anode for Use in Lithium-Ion Batteries. *Small* **2024**, *20*, 2309918. [CrossRef] [PubMed]
81. Cho, J.S.; Hong, Y.J.; Kang, Y.C. Design and Synthesis of Bubble-Nanorod-Structured Fe_2O_3 –Carbon Nanofibers as Advanced Anode Material for Li-Ion Batteries. *ACS Nano* **2015**, *9*, 4026–4035. [CrossRef] [PubMed]
82. Carbone, M. Zn defective $ZnCo_2O_4$ nanorods as high capacity anode for lithium ion batteries. *J. Electroanal. Chem.* **2018**, *815*, 151–157. [CrossRef]
83. Cui, Z.; Wang, S.; Zhang, Y.; Cao, M. High-performance lithium storage of Co_3O_4 achieved by constructing porous nanotube structure. *Electrochim. Acta* **2015**, *182*, 507–515. [CrossRef]
84. Cao, F.-F.; Deng, J.-W.; Xin, S.; Ji, H.-X.; Schmidt, O.G.; Wan, L.-J.; Guo, Y.-G. Cu-Si Nanocable Arrays as High-Rate Anode Materials for Lithium-Ion Batteries. *Adv. Mater.* **2011**, *23*, 4415–4420. [CrossRef]
85. Cheong, J.Y.; Kim, C.; Jung, J.-W.; Yoon, K.R.; Kim, I.-D. Porous SnO_2-CuO nanotubes for highly reversible lithium storage. *J. Power Sources* **2018**, *373*, 11–19. [CrossRef]
86. Xu, J.; Wu, H.; Wang, F.; Xia, Y.; Zheng, G. Zn_4 Sb_3 Nanotubes as Lithium Ion Battery Anodes with High Capacity and Cycling Stability. *Adv. Energy Mater.* **2013**, *3*, 286–289. [CrossRef]
87. Choi, W.; Oh, S.; Hwang, S.; Chae, S.; Park, H.; Lee, W.; Woo, C.; Dong, X.; Choi, K.H.; Ahn, J.; et al. One-dimensional van der Waals transition metal chalcogenide as an anode material for advanced lithium-ion batteries. *J. Mater. Chem. A Mater.* **2024**, *12*, 7122–7131. [CrossRef]
88. Liu, Y.; Zhao, Y.; Jiao, L.; Chen, J. A graphene-like MoS_2 /graphene nanocomposite as a highperformance anode for lithium ion batteries. *J. Mater. Chem. A* **2014**, *2*, 13109–13115. [CrossRef]
89. Wang, B.; Li, X.; Zhang, X.; Luo, B.; Jin, M.; Liang, M.; Dayeh, S.A.; Picraux, S.T.; Zhi, L. Adaptable Silicon–Carbon Nanocables Sandwiched between Reduced Graphene Oxide Sheets as Lithium Ion Battery Anodes. *ACS Nano* **2013**, *7*, 1437–1445. [CrossRef] [PubMed]
90. Mahmood, N.; Zhang, C.; Liu, F.; Zhu, J.; Hou, Y. Hybrid of Co_3 Sn_2 @Co Nanoparticles and Nitrogen-Doped Graphene as a Lithium Ion Battery Anode. *ACS Nano* **2013**, *7*, 10307–10318. [CrossRef]
91. Ni, J.; Zhao, Y.; Li, L.; Mai, L. Ultrathin MoO_2 nanosheets for superior lithium storage. *Nano Energy* **2015**, *11*, 129–135. [CrossRef]
92. Sun, F.; Huang, K.; Qi, X.; Gao, T.; Liu, Y.; Zou, X.; Wei, X.; Zhong, J. A rationally designed composite of alternating strata of Si nanoparticles and graphene: A high-performance lithium-ion battery anode. *Nanoscale* **2013**, *5*, 8586. [CrossRef] [PubMed]
93. Lee, D.G.; Cho, J.Y.; Kim, J.H.; Ryoo, G.; Yoon, J.; Jo, A.; Lee, M.H.; Park, J.H.; Yoo, J.-K.; Lee, D.Y.; et al. Dispersant-Free Colloidal and Interfacial Engineering of Si-Nanocarbon Hybrid Anode Materials for High-Performance Li-Ion Batteries. *Adv. Funct. Mater.* **2024**, *34*, 2311353. [CrossRef]
94. Zhou, M.; Li, X.; Wang, B.; Zhang, Y.; Ning, J.; Xiao, Z.; Zhang, X.; Chang, Y.; Zhi, L. High-Performance Silicon Battery Anodes Enabled by Engineering Graphene Assemblies. *Nano Lett.* **2015**, *15*, 6222–6228. [CrossRef] [PubMed]
95. Chen, Y.; Zhu, J.; Qu, B.; Lu, B.; Xu, Z. Graphene improving lithium-ion battery performance by construction of $NiCo_2O_4$/graphene hybrid nanosheet arrays. *Nano Energy* **2014**, *3*, 88–94. [CrossRef]
96. Fei, L.; Lin, Q.; Yuan, B.; Chen, G.; Xie, P.; Li, Y.; Xu, Y.; Deng, S.; Smirnov, S.; Luo, H. Reduced Graphene Oxide Wrapped FeS Nanocomposite for Lithium-Ion Battery Anode with Improved Performance. *ACS Appl. Mater. Interfaces* **2013**, *5*, 5330–5335. [CrossRef] [PubMed]
97. McNulty, D.; Carroll, E.; O'Dwyer, C. Rutile TiO_2 Inverse Opal Anodes for Li-Ion Batteries with Long Cycle Life, High-Rate Capability, and High Structural Stability. *Adv. Energy Mater.* **2017**, *7*, 1602291. [CrossRef]

98. Yang, S.; Liang, Q.; Wu, H.; Pi, J.; Wang, Z.; Luo, Y.; Liu, Y.; Long, Z.; Zhou, D.; Wen, Y.; et al. Lead-Free Double Perovskite $Cs_2NaErCl_6$: Li^+ as High-Stability Anodes for Li-Ion Batteries. *J. Phys. Chem. Lett.* **2022**, *13*, 4981–4987. [CrossRef] [PubMed]
99. Liu, S.; Zhang, K.; Tan, L.; Qi, S.; Liu, G.; Chen, J.; Lou, Y. All-inorganic halide perovskite $CsPbBr_3$@CNTs composite enabling superior lithium storage performance with pseudocapacitive contribution. *Electrochim. Acta* **2021**, *367*, 137352. [CrossRef]
100. Paul, T.; Maiti, S.; Chatterjee, B.K.; Bairi, P.; Das, B.K.; Thakur, S.; Chattopadhyay, K.K. Electrochemical Performance of 3D Network $CsPbBr_3$ Perovskite Anodes for Li-Ion Batteries: Experimental Venture with Theoretical Expedition. *J. Phys. Chem. C* **2021**, *125*, 16892–16902. [CrossRef]
101. Kaisar, N.; Paul, T.; Chi, P.-W.; Su, Y.-H.; Singh, A.; Chu, C.-W.; Wu, M.-K.; Wu, P.M. Electrochemical Performance of Orthorhombic $CsPbI_3$ Perovskite in Li-Ion Batteries. *Materials* **2021**, *14*, 5718. [CrossRef] [PubMed]
102. Zhang, J.; Li, C.M. Nanoporous metals: Fabrication strategies and advanced electrochemical applications in catalysis, sensing and energy systems. *Chem. Soc. Rev.* **2012**, *41*, 7016–7031. [CrossRef] [PubMed]
103. Zhao, Y.; Liu, B.; Pan, L.; Yu, G. 3D nanostructured conductive polymer hydrogels for high-performance electrochemical devices. *Energy Environ. Sci.* **2013**, *6*, 2856–2870. [CrossRef]
104. Huang, X.; Chen, J.; Lu, Z.; Yu, H.; Yan, Q.; Hng, H.H. Carbon inverse opal entrapped with electrode active nanoparticles as high-performance anode for lithium-ion batteries. *Sci. Rep.* **2013**, *3*, 2317. [CrossRef]
105. Wu, H.; Pi, J.; Liu, Q.; Liang, Q.; Qiu, J.; Guo, J.; Long, Z.; Zhou, D.; Wang, Q. All-Inorganic Lead Free Double Perovskite Li-Battery Anode Material Hosting High Li^+ Ion Concentrations. *J. Phys. Chem. Lett.* **2021**, *12*, 4125–4129. [CrossRef] [PubMed]
106. Pal, P.; Ghosh, A. Three-Dimensional Perovskite Anode for Quasi-Solid-State-Ion and Dual-Ion Batteries: Mechanism of Conversion Process in Perovskite. *Phys. Rev. Appl.* **2020**, *14*, 064010. [CrossRef]
107. Ma, Y.; Xie, X.; Yang, W.; Yu, Z.; Sun, X.; Zhang, Y.; Yang, X.; Kimura, H.; Hou, C.; Guo, Z.; et al. *Recent Advances in Transition Metal Oxides with Different Dimensions as Electrodes for High-Performance Supercapacitors*; Springer Science and Business Media B.V.: Dordrecht, The Netherlands, 2021. [CrossRef]
108. Chen, W.; Zhang, X.; Mo, L.-E.; Zhang, Y.; Chen, S.; Zhang, X.; Hu, L. $NiCo_2S_4$ quantum dots with high redox reactivity for hybrid supercapacitors. *Chem. Eng. J.* **2020**, *388*, 124109. [CrossRef]
109. Wang, Y.; Wang, Y.; Hosono, E.; Wang, K.; Zhou, H. The design of a $LiFePO_4$/carbon nanocomposite with a core-shell structure and its synthesis by an in situ polymerization restriction method. *Angew. Chem. Int. Ed.* **2008**, *47*, 7461–7465. [CrossRef]
110. Fang, T.; Duh, J.-G.; Sheen, S.-R. Improving the Electrochemical Performance of $LiCoO_2$ Cathode by Nanocrystalline ZnO Coating. *J. Electrochem. Soc.* **2005**, *152*, A1701. [CrossRef]
111. Fu, L.J.; Liu, H.; Li, C.; Wu, Y.P.; Rahm, E.; Holze, R.; Wu, H.Q. *Surface Modifications of Electrode Materials for Lithium Ion Batteries*; Elsevier Masson SAS: Amsterdam, The Netherlands, 2006. [CrossRef]
112. Wang, B.; Luo, B.; Li, X.; Zhi, L. Graphene-Inorganic Composites as Electrode Materials for Lithium-Ion Batteries. In *Chemical Synthesis and Applications of Graphene and Carbon Materials*; Wiley: Hoboken, NJ, USA, 2016; pp. 217–249. [CrossRef]
113. Yang, S.; Feng, X.; Ivanovici, S.; Müllen, K. Fabrication of Graphene-Encapsulated Oxide Nanoparticles: Towards High-Performance Anode Materials for Lithium Storage. *Angew. Chem.* **2010**, *122*, 8586–8589. [CrossRef]
114. Yang, S.; Cui, G.; Pang, S.; Cao, Q.; Kolb, U.; Feng, X.; Maier, J.; Mllen, K. Fabrication of cobalt and cobalt oxide/graphene composites: Towards high-performance anode materials for lithium ion batteries. *ChemSusChem* **2010**, *3*, 236–239. [CrossRef] [PubMed]
115. Kim, H.; Seo, D.H.; Kim, S.W.; Kim, J.; Kang, K. Highly reversible Co_3O_4/graphene hybrid anode for lithium rechargeable batteries. *Carbon* **2011**, *49*, 326–332. [CrossRef]
116. Xia, F.; Hu, X.; Sun, Y.; Luo, W.; Huang, Y. Layer-by-layer assembled MoO_2-graphene thin film as a high-capacity and binder-free anode for lithium-ion batteries. *Nanoscale* **2012**, *4*, 4707–4711. [CrossRef]
117. Mai, Y.J.; Tu, J.P.; Gu, C.D.; Wang, X.L. Graphene anchored with nickel nanoparticles as a high-performance anode material for lithium ion batteries. *J. Power Sources* **2012**, *209*, 1–6. [CrossRef]
118. Tao, H.C.; Fan, L.Z.; Mei, Y.; Qu, X. Self-supporting Si/Reduced Graphene Oxide nanocomposite films as anode for lithium ion batteries. *Electrochem. Commun.* **2011**, *13*, 1332–1335. [CrossRef]
119. Cheng, J.; Du, J. Facile synthesis of germanium-graphene nanocomposites and their application as anode materials for lithium ion batteries. *CrystEngComm* **2012**, *14*, 397–400. [CrossRef]
120. Zhu, X.; Zhu, Y.; Murali, S.; Stoller, M.D.; Ruoff, R.S. Nanostructured reduced graphene oxide/Fe_2O_3 composite as a high-performance anode material for lithium ion batteries. *ACS Nano* **2011**, *5*, 3333–3338. [CrossRef] [PubMed]
121. Liu, R.; Cho, S.I.; Lee, S.B. Poly(3,4-ethylenedioxythiophene) nanotubes as electrode materials for a high-powered supercapacitor. *Nanotechnology* **2008**, *19*, 215710. [CrossRef] [PubMed]
122. Nam, K.T.; Kim, D.-W.; Yoo, P.J.; Chiang, C.-Y.; Meethong, N.; Hammond, P.T.; Chiang, Y.-M.; Belcher, A.M. Virus-Enabled Synthesis and Assembly of Nanowires for Lithium Ion Battery Electrodes. *Science* **2006**, *312*, 885–888. [CrossRef] [PubMed]
123. Park, M.; Wang, G.; Kang, Y.; Wexler, D.; Dou, S.; Liu, H. Preparation and Electrochemical Properties of SnO_2 Nanowires for Application in Lithium-Ion Batteries. *Angew. Chem. Int. Ed.* **2007**, *46*, 750–753. [CrossRef]

124. Sides, C.R.; Croce, F.; Young, V.Y.; Martin, C.R.; Scrosati, B. A High-Rate, Nanocomposite $LiFePO_4$/Carbon Cathode. *Electrochem. Solid-State Lett.* **2005**, *8*, A484. [CrossRef]
125. Cho, S.I.; Lee, S.B. Fast Electrochemistry of Conductive Polymer Nanotubes: Synthesis, Mechanism, and Application. *ACC Chem. Res.* **2008**, *41*, 699–707. [CrossRef]
126. Kim, D.K.; Muralidharan, P.; Lee, H.-W.; Ruffo, R.; Yang, Y.; Chan, C.K.; Peng, H.; Huggins, R.A.; Cui, Y. Spinel $LiMn_2O_4$ Nanorods as Lithium Ion Battery Cathodes. *Nano Lett.* **2008**, *8*, 3948–3952. [CrossRef] [PubMed]
127. Yan, J.; Khoo, E.; Sumboja, A.; Lee, P.S. Facile Coating of Manganese Oxide on Tin Oxide Nanowires with High-Performance Capacitive Behavior. *ACS Nano* **2010**, *4*, 4247–4255. [CrossRef] [PubMed]
128. Li, J.; Cui, L.; Zhang, X. Preparation and electrochemistry of one-dimensional nanostructured MnO_2/PPy composite for electrochemical capacitor. *Appl. Surf. Sci.* **2010**, *256*, 4339–4343. [CrossRef]
129. Li, X.; Cheng, F.; Guo, B.; Chen, J. Template-Synthesized $LiCoO_2$, $LiMn_2O_4$, and $LiNi_{0.8}Co_{0.2}O_2$ Nanotubes as the Cathode Materials of Lithium Ion Batteries. *J. Phys. Chem. B* **2005**, *109*, 14017–14024. [CrossRef]
130. Wei, Q.; An, Q.; Chen, D.; Mai, L.; Chen, S.; Zhao, Y.; Hercule, K.M.; Xu, L.; Minhas-Khan, A.; Zhang, Q. One-Pot Synthesized Bicontinuous Hierarchical $Li_3V_2(PO_4)_3$ /C Mesoporous Nanowires for High-Rate and Ultralong-Life Lithium-ion Batteries. *Nano Lett.* **2014**, *14*, 1042–1048. [CrossRef]
131. Zhu, C.; Yu, Y.; Gu, L.; Weichert, K.; Maier, J. Electrospinning of Highly Electroactive Carbon-Coated Single-Crystalline $LiFePO_4$ Nanowires. *Angew. Chem. Int. Ed.* **2011**, *50*, 6278–6282. [CrossRef] [PubMed]
132. Wang, H.; Yang, Y.; Liang, Y.; Cui, L.-F.; Sanchez Casalongue, H.; Li, Y.; Hong, G.; Cui, Y.; Dai, H. $LiMn_1$-xFexPO_4 Nanorods Grown on Graphene Sheets for Ultra-High Rate Performance Lithium Ion Batteries. *arXiv* **2011**, arXiv:1107.0111. [CrossRef]
133. Trinh, D.V.; Nguyen, M.T.T.; Dang, H.T.M.; Dang, D.T.; Le, H.T.T.; Le, H.T.N.; Tran, H.V.; Huynh, C.D. Hydrothermally synthesized nanostructured $LiMn_xFe1-xPO_4$(x = 0 – 0.3) cathode materials with enhanced properties for lithium-ion batteries. *Sci. Rep.* **2021**, *11*, 12280. [CrossRef] [PubMed]
134. Qiao, Y.Q.; Tu, J.P.; Mai, Y.J.; Cheng, L.J.; Wang, X.L.; Gu, C.D. Enhanced electrochemical performances of multi-walled carbon nanotubes modified $Li_3V_2(PO_4)_3$/C cathode material for lithium-ion batteries. *J. Alloys Compd.* **2011**, *509*, 7181–7185. [CrossRef]
135. Su, X.; Wu, Q.; Li, J.; Xiao, X.; Lott, A.; Lu, W.; Sheldon, B.W.; Wu, J. Silicon-Based Nanomaterials for Lithium-Ion Batteries: A Review. *Adv. Energy Mater.* **2014**, *4*, 1300882. [CrossRef]
136. Cui, L.-F.; Ruffo, R.; Chan, C.K.; Peng, H.; Cui, Y. Crystalline-Amorphous Core−Shell Silicon Nanowires for High Capacity and High Current Battery Electrodes. *Nano Lett.* **2009**, *9*, 491–495. [CrossRef] [PubMed]
137. Wu, H.; Chan, G.; Choi, J.W.; Ryu, I.; Yao, Y.; McDowell, M.T.; Lee, S.W.; Jackson, A.; Yang, Y.; Hu, L.; et al. Stable cycling of double-walled silicon nanotube battery anodes through solid–electrolyte interphase control. *Nat. Nanotechnol.* **2012**, *7*, 310–315. [CrossRef] [PubMed]
138. Naguib, M.; Mashtalir, O.; Carle, J.; Presser, V.; Lu, J.; Hultman, L.; Gogotsi, Y.; Barsoum, M.W. Two-Dimensional Transition Metal Carbides. *ACS Nano* **2012**, *6*, 1322–1331. [CrossRef] [PubMed]
139. Eames, C.; Islam, M.S. Ion Intercalation into Two-Dimensional Transition-Metal Carbides: Global Screening for New High-Capacity Battery Materials. *J. Am. Chem. Soc.* **2014**, *136*, 16270–16276. [CrossRef]
140. Naguib, M.; Mochalin, V.N.; Barsoum, M.W.; Gogotsi, Y. 25th Anniversary Article: MXenes: A New Family of Two-Dimensional Materials. *Adv. Mater.* **2014**, *26*, 992–1005. [CrossRef] [PubMed]
141. Naguib, M.; Come, J.; Dyatkin, B.; Presser, V.; Taberna, P.-L.; Simon, P.; Barsoum, M.W.; Gogotsi, Y. MXene: A promising transition metal carbide anode for lithium-ion batteries. *Electrochem. Commun.* **2012**, *16*, 61–64. [CrossRef]
142. Luo, J.; Tao, X.; Zhang, J.; Xia, Y.; Huang, H.; Zhang, L.; Gan, Y.; Liang, C.; Zhang, W. Sn^{4+} Ion Decorated Highly Conductive Ti_3C_2 MXene: Promising Lithium-Ion Anodes with Enhanced Volumetric Capacity and Cyclic Performance. *ACS Nano* **2016**, *10*, 2491–2499. [CrossRef] [PubMed]
143. Luo, J.; Tao, X.; Zhang, J.; Xia, Y.; Huang, H.; Zhang, L.; Gan, Y.; Liang, C.; Zhang, W. Ultra-High-Rate Pseudocapacitive Energy Storage in Two-Dimensional Transition Metal Carbides. In *MXenes*; Jenny Stanford Publishing: New York, NY, USA, 2023; pp. 723–743. [CrossRef]
144. Novoselov, K.S.; Geim, A.K.; Morozov, S.V.; Jiang, D.; Zhang, Y.; Dubonos, S.V.; Grigorieva, I.V.; Firsov, A.A. Electric Field Effect in Atomically Thin Carbon Films. *Science* **2004**, *306*, 666–669. [CrossRef]
145. Chabot, V.; Higgins, D.; Yu, A.; Xiao, X.; Chen, Z.; Zhang, J. A review of graphene and graphene oxide sponge: Material synthesis and applications to energy and the environment. *Energy Environ. Sci.* **2014**, *7*, 1565–1596. [CrossRef]
146. Wei, D.; Haque, S.; Andrew, P.; Kivioja, J.; Ryhänen, T.; Pesquera, A.; Centeno, A.; Alonso, B.; Chuvilin, A.; Zurutuza, A.; et al. Ultrathin rechargeable all-solid-state batteries based on monolayer graphene. *J. Mater. Chem. A Mater.* **2013**, *1*, 3177. [CrossRef]
147. Kim, H.; Park, K.-Y.; Hong, J.; Kang, K. All-graphene-battery: Bridging the gap between supercapacitors and lithium ion batteries. *Sci. Rep.* **2014**, *4*, 5278. [CrossRef] [PubMed]
148. Shu, K.; Wang, C.; Wang, M.; Zhao, C.; Wallace, G.G. Graphene cryogel papers with enhanced mechanical strength for high performance lithium battery anodes. *J. Mater. Chem. A* **2014**, *2*, 1325–1331. [CrossRef]

149. Cohn, A.P.; Oakes, L.; Carter, R.; Chatterjee, S.; Westover, A.S.; Share, K.; Pint, C.L. Assessing the improved performance of freestanding, flexible graphene and carbon nanotube hybrid foams for lithium ion battery anodes. *Nanoscale* **2014**, *6*, 4669–4675. [CrossRef] [PubMed]
150. Hassoun, J.; Bonaccorso, F.; Agostini, M.; Angelucci, M.; Betti, M.G.; Cingolani, R.; Gemmi, M.; Mariani, C.; Panero, S.; Pellegrini, V.; et al. An Advanced Lithium-Ion Battery Based on a Graphene Anode and a Lithium Iron Phosphate Cathode. *Nano Lett.* **2014**, *14*, 4901–4906. [CrossRef]
151. Liu, M.; Yan, C.; Zhang, Y. Fabrication of Nb_2O_5 Nanosheets for High-rate Lithium Ion Storage Applications. *Sci. Rep.* **2015**, *5*, 8326. [CrossRef]
152. Xiao, J.; Choi, D.; Cosimbescu, L.; Koech, P.; Liu, J.; Lemmon, J.P. Exfoliated MoS_2 Nanocomposite as an Anode Material for Lithium Ion Batteries. *Chem. Mater.* **2010**, *22*, 4522–4524. [CrossRef]
153. Qu, B.; Ma, C.; Ji, G.; Xu, C.; Xu, J.; Meng, Y.S.; Wang, T.; Lee, J.Y. Layered SnS_2-Reduced Graphene Oxide Composite—A High-Capacity, High-Rate, and Long-Cycle Life Sodium-Ion Battery Anode Material. *Adv. Mater.* **2014**, *26*, 3854–3859. [CrossRef] [PubMed]
154. Zhang, Y.; Zhu, P.; Huang, L.; Xie, J.; Zhang, S.; Cao, G.; Zhao, X. Few-Layered SnS_2 on Few-Layered Reduced Graphene Oxide as Na-Ion Battery Anode with Ultralong Cycle Life and Superior Rate Capability. *Adv. Funct. Mater.* **2015**, *25*, 481–489. [CrossRef]
155. Prikhodchenko, P.V.; Yu, D.Y.W.; Batabyal, S.K.; Uvarov, V.; Gun, J.; Sladkevich, S.; Mikhaylov, A.A.; Medvedev, A.G.; Lev, O. Nanocrystalline tin disulfide coating of reduced graphene oxide produced by the peroxostannate deposition route for sodium ion battery anodes. *J. Mater. Chem. A Mater.* **2014**, *2*, 8431. [CrossRef]
156. Zhu, F.-F.; Chen, W.-J.; Xu, Y.; Gao, C.-L.; Guan, D.-D.; Liu, C.-H.; Qian, D.; Zhang, S.-C.; Jia, J.-F. Epitaxial growth of two-dimensional stanene. *Nat. Mater.* **2015**, *14*, 1020–1025. [CrossRef] [PubMed]
157. Li, W.; Yang, Y.; Zhang, G.; Zhang, Y.-W. Ultrafast and Directional Diffusion of Lithium in Phosphorene for High-Performance Lithium-Ion Battery. *Nano Lett.* **2015**, *15*, 1691–1697. [CrossRef]
158. Mannix, A.J.; Zhou, X.-F.; Kiraly, B.; Wood, J.D.; Alducin, D.; Myers, B.D.; Liu, X.; Fisher, B.L.; Santiago, U.; Guest, J.R.; et al. Synthesis of borophenes: Anisotropic, two-dimensional boron polymorphs. *Science* **2015**, *350*, 1513–1516. [CrossRef]
159. Tritsaris, G.A.; Kaxiras, E.; Meng, S.; Wang, E. Adsorption and Diffusion of Lithium on Layered Silicon for Li-Ion Storage. *Nano Lett.* **2013**, *13*, 2258–2263. [CrossRef] [PubMed]
160. Jiang, H.R.; Lu, Z.; Wu, M.C.; Ciucci, F.; Zhao, T.S. Borophene: A promising anode material offering high specific capacity and high rate capability for lithium-ion batteries. *Nano Energy* **2016**, *23*, 97–104. [CrossRef]
161. Mahmoud, Z.H.; Ajaj, Y.; Ghadir, G.K.; Al-Tmimi, H.M.; Jasim, H.H.; Al-Salih, M.; Alubiady, M.H.S.; Al-Ani, A.M.; Jumaa, S.S.; Azat, S.; et al. Carbon-doped titanium dioxide (TiO_2) as Li-ion battery electrode: Synthesis, characterization, and performance. *Results Chem.* **2024**, *7*, 101422. [CrossRef]
162. Stein, A.; Wilson, B.E.; Rudisill, S.G. Design and functionality of colloidal–crystal–templated materials—Chemical applications of inverse opals. *Chem. Soc. Rev.* **2013**, *42*, 2763–2803. [CrossRef]
163. Xu, J.; Wang, X.; Wang, X.; Chen, D.; Chen, X.; Li, D.; Shen, G. Three-Dimensional Structural Engineering for Energy-Storage Devices: From Microscope to Macroscope. *ChemElectroChem* **2014**, *1*, 975–1002. [CrossRef]
164. Peng, C.; Chen, B.; Qin, Y.; Yang, S.; Li, C.; Zuo, Y.; Liu, S.; Yang, J. Facile ultrasonic synthesis of coo quantum dot/graphene nanosheet composites with high lithium storage capacity. *ACS Nano* **2012**, *6*, 1074–1081. [CrossRef] [PubMed]
165. Wang, X.; Wu, X.-L.; Guo, Y.-G.; Zhong, Y.; Cao, X.; Ma, Y.; Yao, J. Synthesis and lithium storage properties of Co_3O_4 nanosheet-assembled multishelled hollow spheres. *Adv. Funct. Mater.* **2010**, *20*, 1680–1686. [CrossRef]
166. Wang, J.; Yang, N.; Tang, H.; Dong, Z.; Jin, Q.; Yang, M.; Kisailus, D.; Zhao, H.; Tang, Z.; Wang, D. Accurate control of multishelled Co_3O_4 hollow microspheres as high-performance anode materials in lithium-ion batteries. *Angew. Chem. Int. Ed.* **2013**, *52*, 6417–6420. [CrossRef]
167. Liu, Z.; Mi, J.; Yang, Y.; Li, J.; Tan, X. Synthesis, characterization and electrochemical properties of three-dimensionally ordered macroporous α-Fe_2O_3. *Mater. Sci. Eng. B* **2012**, *177*, 1612–1617. [CrossRef]
168. Kasavajjula, U.; Wang, C.; Appleby, A.J. Nano- and bulk-silicon-based insertion anodes for lithium-ion secondary cells. *J. Power Sources* **2007**, *163*, 1003–1039. [CrossRef]
169. Park, M.-H.; Kim, M.G.; Joo, J.; Kim, K.; Kim, J.; Ahn, S.; Cui, Y.; Cho, J. Silicon nanotube battery anodes. *Nano Lett.* **2009**, *9*, 3844–3847. [CrossRef] [PubMed]
170. Zhang, T.; Fu, L.; Gao, J.; Yang, L.; Wu, Y.; Wu, H. Core-shell Si/C nanocomposite as anode material for lithium ion batteries. *Pure Appl. Chem.* **2006**, *78*, 1889–1896. [CrossRef]
171. Jin, Y.; Munakata, H.; Okada, N.; Kanamura, K. Design and evaluation of a three dimensionally ordered macroporous structure within a highly patterned cylindrical Sn-Ni electrode for advanced lithium ion batteries. *J. Nanomater.* **2013**, *2013*, 937019. [CrossRef]
172. Kim, D.; Suk, J.; Kim, D.W.; Kang, Y.; Im, S.H.; Yang, Y.; Park, O.O. Electrochemically grown three-dimensional porous Si@Ni inverse opal structure for higherperformance Li ion battery anode. *J. Mater. Chem. A* **2014**, *2*, 6396–6401. [CrossRef]

173. Wang, Z.L.; Xu, D.; Wang, H.G.; Wu, Z.; Zhang, X.B. In situ fabrication of porous graphene electrodes for high-performance energy storage. *ACS Nano* **2013**, *7*, 2422–2430. [CrossRef] [PubMed]
174. Lou, S.; Cheng, X.; Zhao, Y.; Lushington, A.; Gao, J.; Li, Q.; Zuo, P.; Wang, B.; Gao, Y.; Ma, Y.; et al. Superior performance of ordered macroporous $TiNb_2O_7$ anodes for lithium ion batteries: Understanding from the structural and pseudocapacitive insights on achieving high rate capability. *Nano Energy* **2017**, *34*, 15–25. [CrossRef]
175. Deng, Z.; Jiang, H.; Hu, Y.; Liu, Y.; Zhang, L.; Liu, H.; Li, C. 3D Ordered Macroporous MoS_2@C Nanostructure for Flexible Li-Ion Batteries. *Adv. Mater.* **2017**, *29*, 1603020. [CrossRef] [PubMed]
176. Liu, X.; Zhao, J.; Hao, J.; Su, B.L.; Li, Y. 3D ordered macroporous germanium fabricated by electrodeposition from an ionic liquid and its lithium storage properties. *J. Mater. Chem. A Mater.* **2013**, *1*, 15076–15081. [CrossRef]
177. Song, T.; Jeon, Y.; Samal, M.; Han, H.; Park, H.; Ha, J.; Yi, D.K.; Choi, J.-M.; Chang, H.; Choi, Y.-M.; et al. A Ge inverse opal with porous walls as an anode for lithium ion batteries. *Energy Environ. Sci.* **2012**, *5*, 9028–9033. [CrossRef]
178. Choi, H.; Takahashi, D.; Kono, K.; Kim, E. Evidence of supersolidity in rotating solid helium. *Science* **2010**, *330*, 1512–1515. [CrossRef] [PubMed]
179. Zhao, N.; Wang, G.; Huang, Y.; Wang, B.; Yao, B.; Wu, Y. Preparation of nanowire arrays of amorphous carbon nanotube-coated single crystal SnO_2. *Chem. Mater.* **2008**, *20*, 2612–2614. [CrossRef]
180. Zhao, N.H.; Yang, L.C.; Zhang, P.; Wang, G.J.; Wang, B.; Yao, B.D.; Wu, Y.P. Polycrystalline SnO_2 nanowires coated with amorphous carbon nanotube as anode material for lithium ion batteries. *Mater. Lett.* **2010**, *64*, 972–975. [CrossRef]
181. Liu, H.; Li, C.; Zhang, H.P.; Fu, L.J.; Wu, Y.P.; Wu, H.Q. Kinetic study on $LiFePO_4$/C nanocomposites synthesized by solid state technique. *J. Power Sources* **2006**, *159*, 717–720. [CrossRef]
182. Kong, F.; Longo, R.C.; Park, M.-S.; Yoon, J.; Yeon, D.-H.; Park, J.-H.; Wang, W.; KC, S.; Doo, S.-G.; Cho, K. Ab initio study of doping effects on $LiMnO_2$ and Li_2MnO_3 cathode materials for Li-ion batteries. *J. Mater. Chem. A* **2015**, *3*, 8489–8500. [CrossRef]
183. Shouji, E.; Buttry, D.A. New Organic-Inorganic Nanocomposite Materials for Energy Storage Applications. *Langmuir* **1999**, *15*, 669–673. [CrossRef]
184. Zhuang, G.V.; Yang, H.; Blizanac, B.; Ross, P.N., Jr. A Study of Electrochemical Reduction of Ethylene and Propylene Carbonate Electrolytes on Graphite Using ATR-FTIR Spectroscopy. *Electrochem. Solid-State Lett.* **2005**, *8*, A441. [CrossRef]
185. Wang, Q.; Wen, Z.; Li, J. A hybrid supercapacitor fabricated with a carbon nanotube cathode and a TiO_2-B nanowire anode. *Adv. Funct. Mater.* **2006**, *16*, 2141–2146. [CrossRef]
186. Ke, Q.; Wang, J. Graphene-based materials for supercapacitor electrodes—A review. *J. Mater.* **2016**, *2*, 37–54. [CrossRef]
187. Yadav, S.; Daniel, S. *Green Synthesis of Zero-Dimensional Carbon Nanostructures in Energy Storage Applications—A Review*; John Wiley and Sons Inc.: Hoboken, NJ, USA, 2024. [CrossRef]
188. Geim, A.K.; Grigorieva, I.V. Van der Waals heterostructures. *Nature* **2013**, *499*, 419–425. [CrossRef]
189. Wang, Z.L. Zinc oxide nanostructures: Growth, properties and applications. *J. Phys. Condens. Matter* **2004**, *16*, R829. [CrossRef]
190. Rolison, D.R.; Long, J.W.; Lytle, J.C.; Fischer, A.E.; Rhodes, C.P.; McEvoy, T.M.; Bour, M.E.; Lubers, A.M. Multifunctional 3D nanoarchitectures for energy storage and conversion. *Chem. Soc. Rev.* **2009**, *38*, 226–252. [CrossRef] [PubMed]

Disclaimer/Publisher's Note: The statements, opinions and data contained in all publications are solely those of the individual author(s) and contributor(s) and not of MDPI and/or the editor(s). MDPI and/or the editor(s) disclaim responsibility for any injury to people or property resulting from any ideas, methods, instructions or products referred to in the content.